INVESTIGATION OF THE INFLUENCE OF SUPERSONIC ROTOR VELOCITIES ON TURBINE PERFORMANCE AND DESIGN

By

Lt. Melville R. Byington, Jr. U. S. Navy

INVESTIGATION OF THE INFLUENCE OF SUPERSONIC ROTOR VELOCITIES ON TURBINE PERFORMANCE AND DESIGN

Lt. Melville R. Byington, Jr. U.S. Navy

Conducted in partial fulfillment of requirements
for the Degree of
AERONAUTICAL AND ASTRONAUTICAL ENGINEER
at the University of Michigan

August, 1963

ACKNOWLEDGMENTS

The author is indebted to Professor R. B. Keller of the University of Michigan and to Professor M. H. Vavra of the United States Naval Postgraduate School for their patient and constructive guidance. Partial cost of this research was borne by the United States Naval Postgraduate School.

TABLE OF CONTENTS

TABLE OF CONTENTS CONT'D

LIST OF TABLES

LIST OF FIGURES

ABSTRACT

An analysis has been conducted of the capabilities of high pressure ratio, single-stage impulse turbines. Some recent experimental work has shown considerable promise for these machines. This work provides a tentative basis for better understanding the potentialities and peculiarities of such high performance turbines.

The present analysis indicates that well designed supersonic-rotor impulse turbines can be expected to produce static efficiencies closely approximating those predicted by well-known (subsonic) curves of static efficiency versus $\frac{\text{blade-speed}}{\text{isentropic jet speed}}$.

Apparently, there presently exists no generally applicable method of blade row loss estimation in the case of supersonic flow. An extension to the Ainley-Mathieson loss prediction procedures to the supersonic case is proposed.

Experimental and estimated supersonic-rotor loss coefficients of the present report differ little in magnitude from well-established results for subsonic blades of similar deflections.

The effect of rotor incidence, in supersonic flow, has a profound influence on pressure and velocity distributions throughout the stage. The effect is inadequately explained by a recently proposed theory. The present analysis proposes an alternative method for estimating the effect.

A logical and straightforward procedure is developed for selection of the "optimum" design point for a single-stage impulse

turbine, given a required RPM, power output, and rotor blade root stress.

The preliminary design of a large rocket-turbine is conducted as an exercise in application of the foregoing developments.

This study was conducted as partial fulfillment of the requirements for the Degree of Aeronautical and Astronautical Engineer at the University of Michigan.

I. INTRODUCTION

In recent years, considerable interest has centered around the development of high pressure ratio turbine stages for rocket-pump drive and other specialized applications. Desirable characteristics are reliability and light weight, with high efficiency as a desirable objective of lesser importance. One type of machine attractive for these applications is the single-stage impulse turbine. This turbine combines low axial thrust on the rotor with potential for high pressure ratios and specific work output. The high pressure ratios normally result in supersonic flow through the rotor, and very few experimental results concerning these stages are available.

The present analysis is undertaken to explore the potentialities of such stages with the benefit of some recent test results. The study is directed along three parallel, but distinct topics. These are: (1) analysis of flow patterns and loss distribution within the stage, (2) development of a scheme for selecting the design point to best achieve specified design goals, and (3) a typical design problem intended to illustrate the results of topics (1) and (2).

II. ANALYSIS OF LOSSES AND FLOW PATTERNS IN SUPERSONIC TURBINE STAGES

1. General Discussion

While a wide body of theoretical and experimental data are available (e.g. Reference 1) for predicting flow patterns and blade losses at low Mach numbers, little information is available at supersonic velocities. As a consequence, turbines designed to operate in these regimes frequently fail to achieve the expected performance and pressure distributions. Two examples are the turbines of Reference 2 and 3 wherein the flow patterns, pressure distributions, and efficiencies differed considerably from estimated design values. In both cases, the results would indicate efficiency was lower than necessary, had the losses been accurately predicted in advance and compensated for in the design geometry.

The method of Reference 4 was utilized by the N.A.S.A. to successfully correlate rotor blade momentum thickness and "specific blade loss" with "blade surface diffusion parameter" for one family of several transonic-rotor turbines. This method does not include the effect of total rotor deflection angle, and has not been satisfactorily generalized. The method predicts a grossly optimistic rotor velocity coefficient for the turbine of Reference 2. The rotor deflection angle is 140° in the latter rotor as compared to only 83° in the N.A.S.A. family, explaining the deviation.

While the loss prediction methods of Reference 1 are comprehensive, they are only recommended by the authors in cases wherein

the flow is everywhere subsonic. Hence, an extension in generality to include supersonic rotor flow is essential to provide for accurate flow channel layout and a more precise estimate of performance.

Figure 1 presents the performance of the two supersonic rotor turbines of Reference 2 and 3, together with that of the N.A.S.A. transonic family of References 5 through 10. For comparison, there are the theoretical curves from References 11 and 12 and an unpublished curve from the Aerojet-General Corp. The theoretical curves presumably are intended to apply to subsonic stages only as no mention is made of Mach number levels. Slight deviations between the curves are explained by minor differences in the geometry and loss assumptions used in deriving them. They may be assumed to fairly approximate the range of efficiencies to be expected for single stage impulse turbines having negligible Mach number effects.

Comparison of these curves with the experimental results of the high performance turbines shows agreement which is enlightening, if not surprising. It seems that no appreciable deterioration in performance may be attributed to Mach effects. The mediocre efficiencies of the turbines of References 2 and 3 are evidently due to very high leaving losses, while the N.A.S.A. family has low leaving losses.

The turbine of Reference 2 shows performance that is quite encouraging when compared to theoretical values. It is no surprise that this is the most recent and probably the most carefully designed of the three. This turbine is designed for high (140^{o}) rotor deflection and maximum static efficiency. On the other hand, the N.A.S.A.

family of turbojet research turbines are designed for high total efficiencies, which average about 85%.

The relatively inferior performance of the turbine of Reference 3 appears to result from causes other than the high Mach number level, although insufficient data are reported to provide for a precise analysis of losses. The performance evidently is degraded by extremely severe flow separation from the rotor suction surface. This explanation is substantiated by the almost negligible change in flow characteristics which resulted from a major modification of the rotor profile. The modification consisted of reducing the blade thickness about 40% by removing metal from the suction surface. The negligible resulting flow change indicates the flow was separated in both cases, and demonstrates the ineffectiveness of profile modifications downstream of the separation point. Since the profile violates the criteria of Reference 13, as discussed in II-5, considerable separation is to be expected. In addition to the separation problem, the design apparently suffers somewhat from relatively large tip clearance and "lap". "Lap" refers to a sudden annulus enlargement immediately downstream of the nozzle exit.

Returning to considerations of the turbine of Reference 2, Figure 1 also illustrates the margin of improvement - about two percentage points in static efficiency - obtained by increasing rotor flare enough to compensate for actual rotor losses. This flare increase allowed design impulse conditions to be closely approached, and illustrates the effect of accurate loss estimates upon geometry and performance. Comparison of theoretical performance

with the best performance of this turbine strongly indicates that any losses associated with supersonic effects must indeed be negligible. This deduction diametrically conflicts with standard works (e.g. Section 4.5 of Reference 1) which indicate a rapid increase in losses as the rotor flow begins to exceed local sonic velocity. Apparently a phenomenon exists which is similar to the "sound barrier" drag increase of aircraft wings. Evidently, when the flow just exceeds local sonic velocity, strong and near-normal shocks exist which cause separation. Once the flow is fully supersonic, the flow field appears to stabilize to the extent that separation losses need be no more severe than in subsonic rotors of similar geometry. The design criteria for minimizing rotor flow separation are considered in II-5. For the present, it seems reasonable to assume that the combined profile, secondary, and tip losses of the supersonic rotor far outweigh any losses credited to supersonic effects.

2. Development of a Method for Loss Prediction in Supersonic Turbine Blading

In view of the foregoing examination of Mach number effects, the loss prediction methods of Reference 1 bear re-examination. The basic Ainley-Mathieson loss parameter is

$$Y \equiv \frac{(\text{Total Inlet Pressure}) - (\text{Total Exit Pressure})}{(\text{Total Exit Pressure}) - (\text{Static Exit Pressure})} .$$

The total pressures are referred to relative and absolute velocities in the rotor and stator cases respectively. Following Reference 1, the total loss coefficient for a blade row, Y_T, is the sum of profile losses,

Y_P, secondary losses, Y_{SEC}, and tip losses, Y_K. Profile losses for stator or rotor blading of arbitrary reaction are empirical functions of solidity, deflection angle, and thickness ratio. Profile losses are easily determined for blades of arbitrary reaction using the methods of Reference 1 with Figures 2a and 2b, which are reproductions of Figures 4a and 4b of Reference 1. In the present case attention is directed only to the special cases of nozzles and impulse rotor blades. In this case the value $\bar{Y}_P$ is determined from Figures 2a or 2b, as appropriate, for standard thickness $\frac{\tau}{c} = .20$. The profile loss estimate for the nozzle or impulse rotor blade in question is then simply

$$Y_P = \frac{\tau/c}{0.20} \bar{Y}_P \qquad (1)$$

The secondary loss equation is developed from relations given in Reference 1. From Equation (4) of Reference 1, there is

$$\lambda = \frac{(C_D)_{sec}}{C_L^2} \left(\frac{s}{c}\right) \qquad (2)$$

From Appendix I, there is $C_L = 2(s/c)\ (\tan\beta_x - \tan\beta_y)\cos\beta_m \qquad (3)$

and

$$(C_D)_{sec} = Y_{sec}\left(\frac{s}{c}\right) \cos^3\beta_m/\cos^2\beta_y \qquad (4)$$

where the vector mean angle,

$$\beta_m \equiv \tan^{-1}\left[\frac{1}{2}\ (\tan\beta_x - \tan\beta_y)\right] \qquad (5)$$

Here β is the gas angle-relative to moving rotor or stationary nozzle as appropriate - and x and y refer to inlet and exit conditions

respectively. Combining 2, 3, and 4, there results

$$Y_{sec} = 4 \frac{\cos^2\beta_y}{\cos\beta_m}(\tan\beta_x - \tan\beta_y)^2 \qquad (6)$$

The coefficient λ is an empirically derived coefficient which accounts for the effect of acceleration on secondary losses. Figure 17 of Reference 1 correlates λ as a function of hub-to-tip radius ratio and $(A_y/A_x)^2$. Since these data were presumably gather for low subsonic velocities, it is assumed $(A_y/A_x)^2 = (W_x/W_y)^2$, where W is relative gas velocity. Based on the foregoing assumption, $(W_x/W_y)^2$ should be an appropriate acceleration parameter independent of M. The assumed variation of λ with acceleration and hub-to-tip ratio is shown as Figure 3. It should be noted that experimental points of the original figure presented considerable scatter, whereas Figure 3 represents a best fit of the data.

The tip clearance loss equation is developed from

$$\frac{(C_D)_K}{C_L^2} = \frac{1}{2} \frac{\Delta h}{h} \Big/ \frac{s}{c} \qquad (7)$$

of Reference 1, page 13. Equation (7) is attributed to Carter, and was developed on a theoretical basis for small deflections. However, Reference 1 points out satisfactory agreement between (7) and tip effects at large deflections, hence the extension seems justified in the absence of a better theory. Similar to (4) above, there is also

$$(C_D)_K = Y_K \left(\frac{s}{c}\right) \frac{\cos^3\beta_m}{\cos^2\beta_y} \qquad (8)$$

Upon combining (3), (7), and (8), there results

$$Y_K = 2\left(\frac{\Delta h}{h}\right) \frac{\cos^2\beta_y}{\cos \beta_m}(\tan \beta_y)^2 \qquad (9)$$

For single stage stators, $\beta_x = 0$ and (9) simplifies to

$$(Y_K)_s = 2\left(\frac{\Delta h}{h}\right) \frac{\sin^2\beta_y}{\cos \beta_m} \qquad (10)$$

Similarly, for impulse rotors with $\beta_x = \beta_y = \beta$, there results

$$(Y_K)_R = 8\left(\frac{\Delta h}{h}\right)\sin^2\beta \qquad (11)$$

The secondary loss relation (6) may also be simplified. In the case of impulse rotors (6) becomes

$$(Y_{sec})_R = 16\lambda \sin^2\beta \qquad (12)$$

In the case of nozzles, Figure 3 indicates that for any practical stator, $\lambda_s = .0055$. Accordingly, (6) becomes

$$(Y_{sec})_s = 4(.0055)\lambda \frac{\sin^2\beta_y}{\cos\beta_m} = .022 \frac{\sin^2\beta_y}{\cos\beta_m} \qquad (13)$$

The stator coefficients, calculated in II-3, tend to be excessively optimistic if (13) is used. Furthermore, the theoretical development based on Reference 1 and leading to (13) has so far made no allowance for effects of blade height on the magnitude of stator secondary losses. However, the data of Figure 15b of Reference 1, as well as Reference 9 and earlier tests, confirms that stator secondary losses are inversely proportional to blade height, while solidity, aspect ratio, and chord have negligible effect on stator losses. In

order to resolve the apparent contradition, (13) has been modified by the coefficient 6/h, chosen empirically based on test results presented in II-3. Hence, the best estimate of stator secondary losses is felt to be

$$(Y_{sec})_s = \frac{.13}{h} \frac{\sin^2\beta_y}{\cos \beta_m} \qquad (14)$$

The total losses of a blading row are determined by addition of the profile, secondary, and tip losses calculated above. That is

$$Y_T = Y_P + Y_{sec} + Y_K \qquad (15)$$

The Ainley-Mathieson loss parameter may be converted to a pressure coefficient or velocity coefficient to simplify subsequent calculations.

One may write

$$Y \equiv \frac{P_x'' - P_y''}{P_y'' - P_y} = \frac{P_x''/P_y'' - 1}{1 - P_y/P_y''} \qquad (16)$$

(note P'' becomes P' in the case of stationary blading). Then

$$C_P \equiv P_y''/P_x'' = \frac{1}{1 + Y[1 - (1 + \frac{\gamma-1}{2} M_y^2)^{-\gamma/\gamma-1}]} \qquad (17)$$

The pressure coefficient is seen to be a function of the relative exit Mach number, M_y, as well as the loss coefficient and gas properties.

The conversion to a velocity coefficient is made using

$$C_P = [1 - \frac{\gamma-1}{2} M_y^2 (\frac{1}{\psi^2} - 1)]^{\frac{\gamma}{\gamma-1}}$$

which is developed in Appendix III of Reference 14. Solving for ψ, there results

$$\psi = \left[1 + \frac{2}{(\gamma-1)M_y^2}\left(1 - C_p^{\frac{\gamma-1}{\gamma}}\right)\right]^{-\frac{1}{2}} \qquad (18)$$

Equations (17) and (18) were programmed on a 7090 computer and the results tabulated in Table I for $\gamma = 1.40$ and $\gamma = 1.25$. The results are also plotted for $\gamma = 1.40$ and appear as Figures 4 and 5.

3. Comparison of Loss Prediction Theory With Available Test Results

The loss prediction theory of II-2 was compared with test results for 7 rotors and 5 stators of experimental turbines. These represent the currently available results that have been published with sufficient information to provide a comparison between predicted and experimental loss coefficients for blading rows. The comparisons covered a moderately wide spectrum of Y, M_y, degree of reaction, deflection angle, solidity, aspect ratio and other parameters. While the volume of test data is quite limited, agreement between theory and experiment is reasonably good. The average deviation between predicted and experimentally determined coefficients is about one percentage point. The precision of both predicted and experimental coefficients is probably no better than plus or minus one point, for reasons discussed below. The comparative results are shown in Table II.

It was necessary to apply certain assumptions and approximations in compiling the data of Table II. The more important of these, with reasons therefore, are:

(a) The N.A.S.A. rotors of Reference 5 through 9 were assumed to have tip clearance $\Delta h/h = .02$ or $\Delta h = .042"$, since clearance was not specified. The errors should be small, as $Y_K < \frac{1}{3} Y_T$ in all cases.

(b) Geometric and velocity characteristics are determined for mean radius conditions, deemed representative of the stage. This assumes that three-dimensional effects are minor.

(c) The effects of Reynolds Number variation are neglected. Reference 1 assumes $(Re)_c = 2 \times 10^5$, while the experimental turbines operated at $(Re)_c$ only 2 to 3 times this value.

(d) The rotor pressure coefficients were not quoted explicitly in References 5 through 9. The coefficients were deduced from

$$(C_P)_R = \frac{P_4''}{P_2''} = \frac{P_4'/P_o'}{(C_P)_s\left[(1-\eta_T) + \eta_T \left(\frac{P_4'}{P_o'}\right)^{\frac{\gamma-1}{\gamma}}\right]^{\frac{\gamma}{\gamma-1}}} \qquad (1)$$

which is developed in Appendix B. While this relation is exact, some interpolation was required to estimate η_T and P_4'/P_o' from the published turbine maps. The stator coefficients were deduced from Reference 9.

4. Comparison of Typical Rotor Velocity Coefficient Estimates Obtained by Different Methods

Figure 6 displays the estimated variation of rotor velocity coefficient, as a function of deflection, for typical impulse blading.

The subsonic reference curve is taken from Reference 12, and represents a mean obtained from a large body of experimental results. The two supersonic curves were obtained following the method of II-2, for a typical geometry. The comparison illustrates several interesting features. The magnitude of the rotor coefficient estimate differs relatively little between the subsonic and supersonic curves. This is not too surprising in view of the comparisons shown in II-1. However, the shape of the supersonic curves at high deflections appears somewhat suspicious, as subsonic experience would anticipate a more rapid deterioration of velocity coefficient. Since there is insufficient test data to confirm or deny the suspicions, one would probably be well advised to use the more conservative estimate, or perhaps a mean. One also notes the increase of ψ_R with M, for fixed losses, Y. This trend is also seen in Figure 5.

5. Detailed Analysis of the Effect of Rotor Profile Geometry on Losses

Reference 13 reports extensive two-dimensional cascade tests of rotor profiles. These tests compared conventional constant-curvature steam turbine profiles to several experimental profiles designed to minimize flow separation in supersonic rotor channels. The inlet Mach number was 1.9 and deflection angle was 140°. Schlieren photographs and total pressure measurements indicated that the resulting "shockless" profiles essentially eliminated shock-induced separation from the suction surface. The over-all velocity coefficient correspondingly increased from .929 to .952.

Reference 2 compared the conventional and shockless profiles in a test turbine, which also operated with several combinations of rotor "lap" and flare. Exact comparison between cascade and turbine tests is difficult due to the limited number of configurations reported. Furthermore, the rotor inlet Mach number was about 1.6 instead of the design value of 1.9. The reduced Mach number resulted from off design nozzle pressure ratio, the reasons for which are discussed in Section II-6.

The maximum rotor velocity coefficient achieved in the turbine was .872. This peak performance was obtained using zero lap, but sufficient flare to approximately compensate for actual losses and approach the design exit flow conditions. In another test, the shockless profile increased total head efficiency about 2-1/2 percentage points, under otherwise identical conditions, while static efficiency changed little if any. These results will be discussed in more detail presently.

The shortcomings of the conventional, constant-curvature passages are thoroughly explored on two-dimensional theoretical grounds in Reference 13. Essentially, it is demonstrated that constant-curvature passages cannot transform a uniform incident flow into a uniform curved flow. Rather, from considerations of a characteristics net, it is evident that the pressure on either surface undergoes a continuous zig-zag pattern of abrupt increases and decreases throughout the length of the curved channel. The pressure rises are expected to react with the thickening boundary layer and produce separation from the suction surface. Cascade tests demonstrated the predicted separation for the conventional profiles.

A second and complementary fault of the conventional profiles is the likelihood of excessive channel width caused by too large a spacing between blades. In supersonic rotor channels, the wider the channel, the larger becomes the uncompensated convex surface acceleration before the compression waves become incident. Hence, an excessively wide spacing produces an increasingly severe pattern of pressure fluctuations. Schlieren photographs also showed a definite tendency toward focusing of the compression "fan" if the spacing were too wide. The abrupt pressure rise triggered separation and flow breakdown. It should be noted that supersonic rotor profiles are determined from channel flow considerations, and solidity is not an appropriate design variable.

The "shockless" profiles of Reference 13 were designed to eliminate the foregoing objections. Their success in cascade tests was mentioned above. An example design is discussed and constructed in Section IV-5 and Figure 15. Essential features of the design scheme are:

(a) Dual curvature, having an entry or transition curvature half as great as the central or mid-chord curvature. The transition curvature extends to a position corresponding to intersections of the first characteristics originating from the opposite surface. Throughout the central region a uniform free vortex flow is theoretically established in planes parallel to the machine axis. A similar transition at the channel exit reconverts the flow

to uniform parallel exit conditions.

(b) A sufficiently small channel width to reduce to acceptable levels the initial, uncompensated acceleration along the convex surface. The maximum recommended width is that prescribed by a transition curvature having

$$\left(\frac{r_i}{r_{out}}\right)_{tran} \geq \cos\left(\sin^{-1}\frac{1}{M_{w_3}}\right) \qquad (1)$$

(c) A channel width sufficiently small to preclude deceleration to sonic velocity along the concave surface. This requirement is generally less stringent than (b), unless the incident Mach number is near unity.

A comparison of cascade tests of the two profiles is seen in Figure 7, where the data were collected from Figures 7 and 19 of Reference 13. Aside from the obvious general superiority of profile B, a closer analysis yields an insight into the nature of the comparative losses. The general spanwise variation of losses indicates the effects of secondary flows, wherein the end wall boundary layers are "centrifuged" toward mid-span by secondary vortices (see Art. 13.7 of Reference 12 for complete discussion). A fair estimate of purely profile losses is probably obtained from the curve peaks, near root (and tip). The greatly increased losses in the central span region point out the predominance of secondary losses -- in qualitative agreement with the estimates of Table II for the rotor

of Reference 2. The spanwise uniform superiority of profile B may be explained by a sharp decrease in profile losses with secondary losses essentially the same in both cases. Hence one concludes that the improvement shown by profile B is due to a reduction in profile losses caused by virtual elimination of shock-induced suction surface separation.

The ratio of losses between the profiles, in cascade, is $(Y_A/Y_B)_{Cascade} = \frac{.63}{.37} = 1.7$, obtained from Figure 5 using the reported velocity coefficients. From Equation III-2-2, static efficiency is directly proportional to $(1 + \psi_R)$ for impulse turbines with all other parameters assumed fixed. Thus, the relative improvement in η due to profile B, if duplicated in the turbine, would be a factor of only

$$\frac{1 + .952}{1 + .929} = 1.012.$$

The reported data of Reference 2 allows at least a rough comparison of losses obtained using profiles A and B in the test turbine. Total efficiencies were .610 and .635 respectively, with only the rotor profiles changed. From Equation II-3-1, $(C_P)_B/(C_P)_A = 1.06$ for stator velocity coefficient and total pressure ratio fixed. Also, using Figure 4 for $M_y \approx 1.4$, together with an estimated $Y_A = .84$ from Table II, one may show $(Y_A/Y_B)_{Rotor} \approx 1.18$. Using Figure 5, the improvement from, say $Y = .84$ to $Y = .84/1.18 = .71$ is equivalent to about .013 increase in ψ_R. Because η is proportional to $(1 + \psi_R)$, it is understandable that the static efficiency improvement, due to the improved rotor profile, was indeed negligible in the test results.

Several important observations may be made from the results of the cascade and turbine tests of the two profiles. It is obvious

that the design features of the shockless profile B prove beneficial in all cases. The relative improvement of profile B is considerably less in the turbine, however, under this single set of test conditions. This result, together with a velocity coefficient reduction from $\psi_{Cascade} = .952$ to $\psi_R = .872$, may be at least partially explained by:

(a) the likelihood of moderate flow separation in the turbine rotor, while virtually none occurred in cascade tests of profile B

(b) the degrading effect of tip losses, not present in cascade, which also are proportionally more detrimental to rotor profile B.

(c) off-design operation of the rotor, which operated at $M_{w_2} = 1.6$ instead of 1.9.

(d) other three-dimensional effects, such as radial pressure gradients, which would be expected to degrade the performance of moving blades.

In addition to the effects of profile changes, Reference 2 also illustrates another important facet of rotor losses and the necessity for their accurate estimation during design. In one test series, an improvement from $\eta = .50$ to .52 and $\psi_R = .844$ to .872 was accomplished by a slight increase in the rotor flare. Both tests used the "shockless" profile. In the first case the flare was based on an estimated $\psi_R = .91$ and, due to the magnitude of the actual losses, the exit swirl angle β_4 was constrained by continuity to be considerably less than its design value. The increased flare approximated actual losses and produced the increased exit swirl and efficiency.

It is evident that an accurate estimate of the actual velocity coefficient may be considerably more important than the questionable ability to increase it a few percentage points.

6. Analysis of the Effects of Rotor Incidence on the Supersonic Flow Through Turbine Blading

On the basis of experiment, Reference 14 concludes that rotor blading with non-zero edge thickness, in supersonic flow having a subsonic axial component, is constrained by continuity to operate at a unique incidence relative to the oncoming gas flow. This incidence determines the gas direction relative to the rotor. Likewise, the absolute discharge angle of the stator, as well as effective stator exit area, is determined uniquely and is virtually independent of the stator geometry. The rotor incidence effect, if uncompensated, can drastically reduce the stator discharge area, pressure ratio, and Mach number. The stator pressure ratio of the test turbine of Reference 2 was reduced to between 1/2 and 2/3 of design value, for example, due to existence of rotor incidence of 4.5°. It is evident care must be taken to estimate the rotor incidence and thus determine the required blading geometry to minimize losses and obtain the desired pressure and velocity distributions.

References 2 and 14 set forth a theory for determining the unique incidence, $i \equiv \beta_2 - \beta_3$. This theory will be stated briefly, and its validity examined, in view of the importance of the incidence.

The incidence is postulated to be that for which the expansion, corresponding to a Prandtl-Meyer turn of $\beta_2 - \beta_3$, is exactly equal to the geometrically available expansion ratio $(s \cos \beta_3 - t)/s\cos \beta_2$.

There is assumed to be a slender wedge leading edge with attached shock, and negligible total pressure loss accompanying the expansion. Hence, the problem as postulated resolves into simultaneous solution of the continuity and Prandtl-Meyer relations.

The Prandtl-Meyer relation in this case simply $\nu + \beta =$ constant or

$$\nu(M_{w_3}) = \nu(M_{w_2}) + (\beta_2 - \beta_3) = \nu(M_{w_2}) + i \qquad (1)$$

A convenient form of the one-dimensional, steady continuity equation may be developed form

$$\rho\, VA = \left(\frac{P}{RT}\right)\left(M\sqrt{\gamma RT}\right) A = \text{constant} \qquad (2)$$

Hence,

$$\frac{PMA}{\sqrt{T}} = \text{constant} \qquad (3)$$

But $T = \dfrac{T''}{1 + \frac{\gamma-1}{2} M_w^2}$ and $P = \dfrac{P''}{\left(1 + \frac{\gamma-1}{2} M_w^2\right)^{\gamma/\gamma-1}}$

Since T'' is constant through a constant diameter rotor,

$$\frac{P''M_wA}{\left(1 + \frac{\gamma-1}{2} M_w^2\right)^{\gamma+1/2(\gamma-1)}} = \text{constant} \qquad (4)$$

Examining stations (see Figure 9) 2 and 3, just upstream and downstream of the leading edge, one writes

$$\frac{A_3}{A_2} = \frac{P_2''}{P_3''} \frac{M_{w_2}}{M_{w_3}} \left(\frac{1 + \frac{\gamma-1}{2} M_{w_3}^2}{1 + \frac{\gamma-1}{2} M_{w_2}^2}\right)^{\gamma+1/2(\gamma-1)} \qquad (5)$$

From the blading geometry, there is also

$$\frac{A_3}{A_2} = \frac{\cos \beta_3 - t/s}{\cos \beta_2} \tag{6}$$

Using $C_p \equiv P_3''/P_2''$ and combining (5) and (6), there results

$$\frac{t}{s} = \cos \beta_3 - \frac{\cos \beta_2}{C_P} \frac{M_{w_2}}{M_{w_3}} \left(\frac{1 + \frac{\gamma-1}{2} M_{w_3}^2}{1 + \frac{\gamma-1}{2} M_{w_2}^2}\right)^{\gamma+1/2(\gamma-1)} \tag{7}$$

Equations (1) and (7) may be solved for two unknowns. Typically, one knows M_{w_2}, β_3, and t/s and wishes to find M_{w_3} and β_2. The incidence is thus determined for a specified incident Mach number and rotor blade profile.

Reference 14 illustrates the theory for an example rotor having $\beta_3 = 70^\circ$ and $M_{w_2} = 1.9$. Reference 2 compared estimated and experimentally deduced incidence, with fair agreement, for $\beta_3 = 70^\circ$ and $M_{w_2} = 1.61$. See Figure 8. Isentropic conditions are assumed throughout.

Upon close scrutiny, however, the above theory may be shown to become absurd as the rotor blade angle, β_3, is reduced somewhat. The anomaly is easily demonstrated by a simple numerical example.

Suppose the (relative) incident flow occurs at $M_{w_2} = 1.6$. The corresponding Prandtl-Meyer angle for $\gamma = 1.4$ is $\nu_2 = 14.9^\circ$. Further suppose a fixed incidence of any reasonable magnitude, say 3°. Now using Equations (1) and (7), calculate the allowable edge thickness t/s, for various β_3. Assume isentropic conditions, $C_p = 1.0$.

By (1), $\nu_3(M_{w_3}) = 17.9^\circ$ which yields a corresponding $M_{w_3} = 1.703$. Equation (7) becomes

$$t/s = \cos \beta_3 - \cos (\beta_3 + 3^\circ) \frac{1.60}{1.703} \left[\frac{1 + .2(1.703)^2}{1 + .2(1.60)^2}\right]^3$$

$$= \cos \beta_3 - 1.075 \cos (\beta_3 + 3^\circ) \qquad (8)$$

For $\beta_3 = 70^\circ$, $t/s = .027$. However, upon reducing β_3 it is seen that t/s decreases monotonically until $t/s = 0$ for $\beta_3 = 52^\circ$. The same conclusions are reached regardless of the selected numerical values. In particular, it is evident that breakdown occurs at even larger β_3 if $C_p < 1.0$ or $M_{w_3} > 1.6$.

The physical explanation of the breakdown of the theory is that, at sufficiently small blade angles, the turned and accelerated Prandtl-Meyer flow (assumed) fails to encounter the requisite geometric expansion necessary to satisfy continuity. In addition to the foregoing arguments, it is also evident that the isentropic, irrotational Prandtl-Meyer flow assumptions cannot hold in an actual turbine rotor. In article 9.10 of Reference 12, Vavra has pointed out the inherent danger in applying two dimensional analysis to such three dimensional flows.

Aside from the merits of the foregoing theory, rotor incidence remains a physical reality with very important implications. Hence, a more satisfactory explanation of its nature must be sought out.

One must agree the continuity relation (7) is valid. Having decided the Prandtl-Meyer relation is not applicable in this case, there remains one more unknown than available equations.

Expanding the Mach number term of (7) in a binomial series, it may be shown that

$$\frac{M_{w_2}}{M_{w_3}}\left(\frac{1+\frac{\gamma-1}{2}M_{w_3}^2}{1+\frac{\gamma-1}{2}M_{w_2}^2}\right)^{\gamma+1/2(\gamma-1)} = 1+\epsilon\left(\frac{\gamma+1}{2}M_{w_2}^2-1\right)+\theta(\epsilon^2)+\ldots$$

where $\epsilon \equiv \frac{M_{w_3}}{M_{w_2}} - 1.$

Substituting in (7), there results

$$t/s = \cos\beta_3 - \frac{1+\epsilon\left(\frac{\gamma+1}{2}M_{w_2}^2-1\right)}{C_P}\cos\beta_2 \qquad (9)$$

From (9) it is evident that for moderate incident Mach numbers, the magnitude of the incidence is relatively insensitive to small differences between M_{w_3} and M_{w_2}.

Equation (9) was compared with the experimentally deduced incidence of Reference 2. For design speed conditions, one is able to deduce $C_P/(1+1.9\epsilon) = .84$. Assuming $\epsilon \geq 0$, one then concludes that

$$.84 \leq C_P \leq 1.00 \quad ; \quad 0 \leq \epsilon \leq .10 .$$

As stated earlier, a second valid equation in the unknowns is apparently lacking. Since it seems probable $\epsilon \ll 1$ in cases of interest, one might assume $\epsilon = 0$ and rewrite Equation (9) as

$$\frac{t}{s} \approx \cos\beta_3 - \frac{\cos\beta_2}{C_P} \qquad (10)$$

The theoretical incidence of Equation (10) and of Reference 14 was compared with the experimental incidence of Reference 2. The comparison is shown in Figure 8. There is fair agreement, at the

design point, between the theoretical estimates for isentropic conditions. Furthermore, Equation (10) is seen to agree with experiment for $C_P = .84$ at design speed and .90 at zero speed. This trend seems reasonable and agrees with the expectations of the authors of Reference 2. Higher relative losses at design speed are attributed to the reduced Mach number with correspondingly stronger, and possibly detached, shocks.

By examining the design speed case further, one may deduce the apparent proportion of total rotor loss, occurring at the leading edge, which results in the 4.5° observed incidence. Over-all rotor losses were reported as $\psi_R = .872$. Using Figure 5, this loss corresponds to $(Y_T)_R = 1.12$. Similarly, from Figure 4 the apparent leading edge loss, $C_P = .84$, corresponds to $(Y_{LE})_R = .25$. Hence, the apparent ratio of leading edge to total rotor loss is $.25/1.12 = 2/9$. As noted above, this apparent ratio represents an upper limit of actual leading edge losses and, in effect, incorporates the effect of any flow acceleration, ϵ, which may occur at the rotor entrance. From Equation (10), for a given blade (or gas) angle and incidence, leading edge losses would be expected to increase with t/s. The foregoing considerations are utilized to estimate incidence in the design problem of IV-5.

The result of a single experiment hardly constitutes a reliable design rule. However, there is provided a reasonably consistent account of the interaction between gas angles, blade angles, and rotor geometry. As mentioned previously, care must be taken to

accurately estimate incidence and preclude serious rotor-stator mismatching with resulting losses. One test cited in Reference 2 clearly indicates the criticality of the problem. Rotor blades having negligible edge thickness were run. During the course of the test, the nozzle pressure ratio decreased from 16/1 to 13/1, corresponding to the accumulation of only a thin carbon deposit on the rotor blades. Nevertheless, the buildup caused the incidence to evidently increase some 2° in order to produce the observed effect.

III. A RATIONAL TECHNIQUE FOR DESIGN POINT SELECTION FOR SINGLE-STAGE IMPULSE TURBINES

1. General Discussion

Given a design goal in terms of RPM and power required, expansion ratio, working fluid, and thermodynamic inlet properties, one is faced with the task of selecting a design point to satisfy the requirements. Literally an infinite number of design points, in terms of blade speed and gas angles, can meet the requirements. Hence, the designer must choose the most desirable combination of high efficiency, compact size and weight, and tolerable stress limits. An obvious approach is a trial and error process. This results in laborious calculations of debatable final success in determining the "best" design point.

A single-stage turbine, especially one with a high expansion ratio, will tend to have sizeable leaving losses. Hence, efficiency is determined primarily by blade to isentropic jet ratio as seen in Figure 1, while the blade speed is limited by material stress considerations. Experience and the mission requirements generally dictate desirable blade materials and allowable stresses. Thus one might be well advised to restrict the infinite number of possible design points to only those which satisfy some specified blade root stress. One could then proceed to decide upon a desirable size, weight, and efficiency combination to meet design requirements.

The following method is one way of logically deciding upon the "best" design point. It requires neither machine calculations

nor infinite human patience. The technique is applicable to single-stage impulse turbines, totally independent of Mach number levels. The loss coefficients which enter may be estimated by any means whatsoever, and are not related necessarily to loss prediction methods of II-2. The nomenclature of the development is defined in Appendix A. The method is applied to a design problem in IV.

2. Static Efficiency as a Function of Velocity Coefficients and Rotor Deflection

In terms of Figure 9, Euler's Turbine Equation may be expressed as

$$\eta = 2 \frac{U}{C_o^2} (W_2 \sin \beta_2 + W_4 \sin \beta_4) \qquad (1)$$

For symmetrical impulse blading of the present case,

$$\beta_2 = \beta_4 = \beta \qquad \text{and} \qquad W_4 = \psi_R W_2$$

Equation (1) may be rewritten,

$$\eta = 2 \frac{U}{C_o^2} (1 + \psi_R) W_2 \sin \beta_2$$

or

$$\eta = 2 \frac{U}{C_o} \frac{W_2}{C_o} (1 + \psi_R) \sin \beta \qquad (2)$$

By definition, $\psi_s \equiv V_2/C_o$, and (2) may be expressed

$$\eta = 2\psi_s^2 (1 + \psi_R) \Theta \delta \sin \beta \qquad (3)$$

From the geometry of Figure 9,

$$\Theta = \sqrt{1 - \delta^2 \cos^2\beta} - \delta \sin \beta \qquad (4)$$

Hence (3) may be expressed

$$\eta = 2\psi_s^2 (1 + \psi_R) \sin\beta \; \delta(\sqrt{1 - \delta^2\cos^2\beta} - \delta\sin\beta) \qquad (5)$$

ψ_R is a known function of both β and δ, in general. ψ_s is independent of δ, but weakly dependent on β - through α_2. Equation (5) allows calculation of efficiency for selected design point coordinates δ, β. While Equation (5) might be considered to "organize" the search for a suitable design point, it places no restriction on the blade stresses.

Incidentally, Equation (5) also illustrates the relative importance of ψ_s as compared to ψ_R. For example, a one percentage point improvement in ψ_s should be roughly equivalent to a four point improvement in ψ_R, since $\psi_s \approx \psi_R \approx 1$.

3. Limiting Stress Requirement

For a selected blading material of a specified taper ratio, including constant cross section blading as a special case, one may show that blade root stress is proportional to the product of radial acceleration and blade height. If bending stresses are neglected,

$$\sigma \sim h \frac{U^2}{R} \qquad (6)$$

By continuity, the mass flow rate is,

$\overset{o}{W}$ = density x axial velocity x annular area, or

$$\overset{o}{W} \sim \rho_4 W_4 \cos\beta \; Rh \qquad (7)$$

The exit density, ρ_4, depends on pressure and temperature at the blade exit. The pressure may be assumed independent of the variables and equal to exhaust pressure, provided the axial component of

velocity is subsonic. The temperature will vary somewhat with $\eta = \eta\ (\delta,\beta)$. If one neglects this variation, Equation (7) becomes

$$\overset{o}{W} \sim W_4 \cos \beta\ Rh \tag{8}$$

For fixed power output, $\overset{o}{W} \sim \frac{1}{\eta}$. Since $W_4 = \psi_R W_2$, Equation (8) becomes

$$\frac{1}{\eta} \sim \psi_R\, W_2 \cos \beta\ Rh \tag{9}$$

Substituting,

$$h \sim \frac{1}{\eta \psi_R\, W_2 R \cos \beta}$$

into (6), there results

$$\sigma \sim (\frac{U}{R})^2 \frac{1}{\eta \psi_R\, W_2 \cos \beta} \tag{10}$$

One notes that U/R, the angular velocity, is fixed in the present case. Further, letting $W_3 \equiv \delta\, V_3 \sim \delta$, by assuming V_3 independent of δ and β, Equation (10) becomes

$$\delta \sim \frac{1}{\eta \psi_R \cos \beta}$$

or

$$\underline{\sigma \eta \psi_R\, \delta \cos \beta \equiv B = \text{constant}} \tag{11}$$

The parameter B has stress units and may be viewed as an invariant property of the particular design specifications and working fluid. Experience indicates that B is indeed virtually constant over quite

a sizeable range of δ, β variation, as illustrated in IV.

If one now selects a specific working stress $\bar{\sigma}$ as a design objective, there results $D \equiv \frac{B}{\bar{\sigma}} = \eta\psi_R \delta \cos\beta$ (12)
Thus, for a specified stress, the parameter D is a unique constant. Furthermore, any design point satisfying (12) automatically satisfies the imposed stress requirement, $\bar{\sigma}$.

4. Combination of Performance and Stress Requirements

By combining the results of Equation (5) and (12),

$$2\psi_s^2(1 + \psi_R) \sin\beta \; \delta(\sqrt{1 - \delta^2\cos^2\beta} - \delta\sin\beta) = \frac{D}{\psi_R \delta\cos\beta} \quad (13)$$

or

$$\delta^2(\sqrt{1 - \delta^2\cos^2\beta} - \delta\sin\beta) = \frac{D}{2\psi_s^2 \psi_R(1 + \psi_R)\sin\beta\cos\beta} \quad (14)$$

For convenience, one may define parameters

$$F' \equiv \frac{D}{2\psi_s^2 \psi_R(1 + \psi_R)\sin\beta\cos\beta} \quad (14a)$$

$$F'' = \delta^2(\sqrt{1 - \delta^2\cos^2\beta} - \delta\sin\beta) \quad (14b)$$

Note that F'' is a universal function of δ and β and could be tabulated.

Since $\psi_R = \psi_R(\delta, \beta)$ and ψ_s is assumed independent of β, while D is a known constant (for a specified $\bar{\sigma}$), one may evaluate Equation (14). There remains an unlimited number of admissible δ, β coordinates which are known to satisfy the imposed stress limit. The problem is the selection of the most attractive δ, β that represents a final design point decision.

As an aid in this decision one might examine some variable additional relationships.

For example, from (13),

$$\eta(\delta,\beta) = \frac{D}{\psi_R \delta \cos \beta} \tag{15}$$

The rotor relative Mach number variation may be examined by noting,

$$M_{w_2} \equiv \frac{W_2}{\sqrt{\gamma R T_2}} = \frac{\delta V_2}{\sqrt{\gamma R T_2}}$$

Furthermore, if $V_2 = \psi_s C_o$ is independent of β, as previously assumed, it follows that T_2 is likewise constant. Hence one notes,

$$M_{w_2} \sim \delta \tag{16}$$

Variation in radius is simply determined from

$$U \sim R \sim \theta \tag{17}$$

Reference 15 gives a useful empirical estimate for single-stage rocket-turbine weight as

$$m,\text{lb.} = 70\pi\,(R,\text{ft.})^2 = 1.53\,(R,\text{in.})^2 \tag{18}$$

Finally, since $\sigma \sim Rh \sim \theta h$, for constant RPM, blade height variation may be deduced from

$$\frac{h\theta}{\sigma} = \text{constant} \tag{19}$$

5. Procedure for Application

Given power and RPM requirements, together with available expansion ratio and turbine inlet conditions for a specified working

fluid, one may proceed in an orderly manner to select the "best" design point, as follows:

(A) Based on experience and operational objectives, one makes a tentative selection of blade material and one or more values of allowable centrifugal blade root stress.

(B) A trial design point is selected in terms of an arbitrary velocity triangle. As a minimum, one evaluates, for the trial design point:

η	ψ_R
$\overset{o}{W}$	β
σ	M_{w_2}
R	M_{w_4}
h	θ
ψ_s	δ

A single calculation of this type should suffice provided the calculated stress is within, say $\pm$ 50 percent of the selected values, $\bar{\sigma}$.

(C) Calculate the invariant B - Equation (III-4-11).

(D) Calculate D corresponding to selected $\bar{\sigma}$ - Equation (III-4-12).

(E) Plot F' against β (for a reasonable regime of β) - Equation III-4-14a. Consider ψ_s constant as calculated in step (b). Consider $\psi_R = \psi_R(\beta, M_{w_4}) \approx \psi_R(\beta)$, using constant M_{w_4} as calculated in step (b). The

curves F' then represent constant stress lines. See Figure 10 for an example.

(F) Plot F'' against β, for selected δ = constant - Equation II-4-14b. Intersections of the constant δ and constant $\bar{\sigma}$ curves determine unlimited compatible (δ, β, $\bar{\sigma}$) design point possibilities.

(G) For any desired (δ, β, $\bar{\sigma}$), calculate:

η	-	Equation (III-4-15)
M_{w_2}	-	Equation (III-4-16)
θ	-	Equation (III-4-4)
R	-	Equation (III-4-17)
U	-	Equation (III-4-17)
m	-	Equation (III-4-18)
h	-	Equation (III-4-19)

(H) As an additional aid in visualizing the variations, plot η against β for $\bar{\sigma}$ = constant. The addition of δ = constant and θ = constant points provides for ready visualization of the variation in η, M_{w_2}, θ, R, U, m, and h along the constant stress curve. See Figure 11.

(I) From the plot of (H), one may then select the most attractive combination of features to fix the design point (δ, β, $\bar{\sigma}$). Estimate η, M_{w_3}, θ, R, U, m, and h for the selected design point. Repeat (B) to verify the estimates above. One notes that the approximations introduced into the technique are now discarded. A second iteration of (C) through (I) would appear unnecessary unless (I) indicates intolerable lack of agreement between the rough and smooth design point estimates.

IV. ILLUSTRATIVE DESIGN PROBLEM

1. Specifications and General Design Philosophy

An example of a preliminary design is presented to illustrate the application of previously discussed methods of loss prediction and design point selection. The specifications and gas properties arbitrarily chosen are those which might correspond to turbodrive requirements of a large liquid propellant rocket using reasonably energetic chemical propellants.

Assumed output requirements are: 28,800 SHP at 15,000 RPM.

Assumed gas properties are:

molecular weight,	$\mathfrak{M}$	=	12.0 lb/mole
specific heat ratio,	γ	=	1.25
constant pressure specific heat	c_p	=	.827 Btu/lb-$^{\circ}$R
total inlet pressure	P'_o	=	450 psia
exhaust static pressure	P_4	=	30 psia
gas constant,	$\bar{R}$	=	128.8 ft-lb/lb-$^{\circ}$R
total inlet temperature,	T'_o	=	2200°R .

The turbine is to be of the single-stage, impulse type to minimize axial thrust on the rotor bearings. A reasonable compromise between static efficiency, size and weight, and simplicity is to be achieved.

2. Design Point Selection

The design point selection method described in Section III is to be followed. A single, arbitrary trial design point serves as a basis for selection of the final design point.

The available isentropic energy is,

$$\Delta H_{IS} = C_P T_o' \left[1 - \left(\frac{P_4}{P_o'}\right)^{\gamma-1/\gamma}\right] = .827 \times 2200 \left[1 - \left(\frac{30}{450}\right)^{.20}\right] = \underline{760 \frac{Btu}{lb}}$$

The isentropic jet velocity,

$$C_o = \sqrt{2gJ\Delta H_{IS}} = \sqrt{5 \times 10^4 \times 760} = \underline{6160 \text{ ft/sec}}$$

The isentropic Mach number,

$$(M_2)_{IS} = \sqrt{\frac{2}{\gamma-1}\left[\left(\frac{P_o'}{P_4}\right)^{\gamma-1/\gamma} - 1\right]} = \sqrt{8\left[15^{.20} - 1\right]} = \underline{2.40}$$

The subsequent steps correspond to those of Section III-5.

STEP A

Suppose consideration be given to blade root stresses of 30,000, 37,500, and 45,000 psia. Most suitable blading materials are known to have densities of about 0.30 lb/in^3.

STEP B

For the first trial arbitrarily select $\alpha_2 = 65^o$, $U/C_o = .3$. From Figure 1, the expected efficiency is $.60 < \eta < .67$. The mean blade speed is, $U = .3 \times 6160 = 1848$ ft/sec. The mean blade radius is

$$R = \frac{1848 \times 60}{2\pi \times 15000} \times 12 = \underline{14.1"}$$

(1) Determination of Stator Velocity Coefficient, ψ_s-

The mass flow rate is

$$\overset{\circ}{W} = \frac{SHP \times \frac{550}{778}}{\eta \Delta H_{IS}} \approx \frac{28800 \times .707}{.64 \times 760}$$

The annulus area,

$$A_2 = 2\pi R h_2 = \frac{\overset{\circ}{W}}{\rho_2 V_{ax,2}} = \frac{\overset{\circ}{W}}{\frac{P_2}{\bar{R}T_2} \psi_s C_o \cos\alpha_2}$$

$$h_2 = \frac{\overset{\circ}{W} \bar{R} T_2}{\psi_s P_2 C_o \cos\alpha_2 2\pi R}$$

For an estimated $\psi_s \approx .95$.

$$T_2 = T_o' - \psi_s^2 \frac{\Delta H_{IS}}{C_P} = 2200 - .95^2 \frac{760}{.827} = 1370^\circ R$$

and

$$h_2 \approx \frac{42 \frac{lb}{sec} \times 128.8 \frac{ft\text{-}lb}{lb\text{-}^\circ R} \times 1370^\circ R}{.95 \times 30 \frac{lb}{in^2} \times 6160 \frac{ft}{sec} \cos 65^\circ \times 2\pi \times 14.1 \text{ in}} = \underline{\underline{1.12"}},$$

approximate annulus height.

The nozzle secondary losses are calculated from Equation (II-2-14),

$$(Y_{sec})_s = \frac{.13}{h_2} \frac{\sin^2\alpha_2}{\cos \alpha_m}$$

where

$$\alpha_m \equiv \tan^{-1} (\tfrac{1}{2} \tan \alpha_2) = \tan^{-1} (\frac{\tan 65^\circ}{2}) = 47^\circ$$

Thus

$$(Y_{sec})_s = \frac{.13}{1.12} \frac{\sin^2 65^\circ}{\cos 47^\circ} = \underline{.14}$$

Stator profile losses are estimated from Figure 2a to be $(Y_p)_s = .06$. Total stator losses, $(Y_T)_s = (Y_{sec})_s + (Y_p)_s \approx .20$. From Table I-d, for $M_2 \approx 2.2$, the velocity coefficient estimate is $\psi_s = .974$.

(2) Determination of some velocity triangle components - See Figure 9.

$$V_2 = \psi_s C_o = .974 \times 6160 = 6000 \text{ ft/sec}$$

$$V_{ax,2} = V_2 \cos \alpha_2 = 6000 \cos 65^\circ = 2535$$

$$\beta_2 = \tan^{-1}\left(\frac{V_2 \sin \alpha_2 - U}{V_{ax,2}}\right) = \tan^{-1} \frac{5435}{2535} = 54.7^\circ$$

$$W_2 = \frac{V_{ax,2}}{\cos \beta_2} = \frac{2535}{\cos 54.7^\circ} = 4390$$

$$\delta \equiv W_2/V_2 = 4390/6000 = .732$$

$$\theta \equiv U/V_2 = 1848/6000 = .308$$

$$T_2 = T_o' - \psi_s^2 \frac{\Delta H_{IS}}{C_P} = 2200 - .974^2 \frac{760}{.827} = 1328^\circ R$$

Revised $$M_2 = \frac{V_2}{\sqrt{\gamma g \bar{R} T_2}} = \frac{6000}{72.0\sqrt{1328}} = 2.29$$

$$M_{w_2} = \frac{W_2}{72.0\sqrt{T_2}} = \frac{4390}{2620} = 1.675$$

(3) Determination of rotor velocity coefficient, ψ_R

Rotor secondary losses are, using Equation (II-2-12), and estimating $\lambda = .03$ from Figure 3,

$$(Y_{sec})_R = .48 \sin^2 \beta_2 = .48 \sin^2 54.7^\circ = .32$$

Tip losses, assuming $\Delta h/h = .03$, from Equation (II-2-11)

$$(Y_K)_R = 8.0 \frac{\Delta h}{h} \sin^2\beta_2 = 8.0 \times .03 \sin^2 54.7^\circ = \underline{.16}$$

Profile losses are estimated from Figure 2b, $(Y_P)_R \approx \underline{.12}$

Estimated total rotor losses are $(Y_T)_R = \underline{.60}$.

With an estimated rotor exit Mach number $M_{W_4} \approx 1.6$, the estimated velocity coefficient from Table I-d is $\psi_R = \underline{.904}$.

The rotor coefficient compares with an estimated $\psi_R = .898$ from the subsonic reference curve of Figure 6 for $\beta = 54.7^\circ$.

(4) Completion of velocity triangle and performance calculations

$$W_4 = \psi_R W_2 = .904 \times 4390 = \underline{3970}$$

$$\beta_4 = \beta_2 = \underline{54.7^\circ}$$

$$V_{ax,2} = W_4 \cos\beta_4 = \underline{2290}$$

$$V_4 = \sqrt{V_{ax,4}^2 + (W_4 \cos\beta_4 - U)^2} = \underline{2680}$$

$$\alpha_4 = \cos^{-1}\left(\frac{V_{ax,4}}{V_4}\right) = \cos^{-1}\left(\frac{2290}{2680}\right) = \underline{31.3^\circ}$$

work output, $W = \dfrac{U\Delta V_u}{gJ} = \dfrac{UW_2(1+\psi_R)\sin\beta_2}{gJ} = \dfrac{1848 \times 4390 \times 1.904 \sin 54.7^\circ}{2.5 \times 10^4}$

$W = 504$ Btu/lb.

Static efficiency, $\eta = \dfrac{W}{\Delta H_{IS}} = \dfrac{504}{760} = \underline{.663}$

This estimate appears reasonable compared with Figure 1.

(5) Temperatures, annulus (rotor blade) heights, and rotor blade stress

Since total relative temperature is constant through the rotor of constant mean radius,

$$T_2'' = T_2 \frac{W_2^2}{2gJC_P} = T_4 + \frac{W_4^2}{2gJC_P} = T_4''$$

Since

$$W_4 \equiv \psi_R W_2, \quad T_4 = T_2 + \frac{W_2^2}{2gJC_P}(1 - \psi_R^2) = 1328 + \frac{4390^2}{4.13 \times 10^4}(1 - .904^2)$$

$$T_4 = \underline{1413^\circ R} \qquad M_{W_4} = \frac{W_4}{720\sqrt{T_4}} = \underline{1.45}$$

and $T_4' = T_4 + \frac{V_4^2}{2gJC_P} = 1413 + \frac{2680^2}{4.13 \times 10^4} = \underline{1589^\circ R}$

Check work output, $W = c_P \Delta T' = .827\ (2200 - 1589) = \underline{505\ \text{Btu/lb.}}$

This constitutes a check for consistency of the velocity and temperature distributions.

The mass flow,

$$\overset{\circ}{W} = \frac{\frac{550}{778}\,\text{SHP}}{W} = \frac{.707 \times 28800}{504} = \underline{40.4\ \text{lb/sec}}$$

The annulus, or rotor leading edge, height is $h_2 = \frac{\overset{\circ}{W}\,\bar{R}\,T_2}{2\pi R P_2 V_{ax,2}}$

$$h_2 = \frac{40.4 \times 128.8 \times 1328}{2\pi \times 14.1 \times 30 \times 2535} = \underline{1.024"}$$

$$h_4 = \frac{\overset{\circ}{W}\,\bar{R}\,T_4}{2\pi\, RP_4 V_{ax,4}} = h_2 \frac{T_4}{T_2}\frac{1}{\psi_R} = 1.024 \times \frac{1413}{1328} \times \frac{1}{.904} = \underline{1.207"}$$

The blade root stress is calculated assuming a blade of height h_4 and density .30 lb/in^3. The centrifugal stresses only are considered, as bending stresses are expected to represent a small fraction of total root stress.

The root force, $F = ma = (\rho A_c \frac{h_4}{g} \frac{\text{lb-sec}^2}{\text{ft}}) (\frac{R}{12} \omega^2 \text{ ft/sec}^2)$

$$F = \rho A_c \frac{h_4}{g} \frac{R}{12} (\frac{2\pi\ 15000}{60})^2$$

$$\sigma = F/A_c = \rho \frac{h_4}{g} \frac{R}{12} (\frac{30000\ \pi}{60})^2 = \underline{1910\ h_4 R \text{ psi}}$$

for $h_4 = 1.207"$ and $R = 14.1"$, $\sigma = \underline{32600 \text{ psi}}$

(6) Summary of step (B) results

η	= .663	ψ	= .904
$\overset{\circ}{W}$	= 40.4 lb/sec	β	= 54.7°
σ	= 32600 psi	M_{w_3}	= 1.675
R	= 14.1"	M_{w_4}	= 1.45
h	= 1.207"	θ	= .308
ψ_s	= .974	δ	= .732

STEP C

$B \equiv \sigma\eta\psi_R \delta \cos\beta = \underline{8250 \text{ psi}}$, the invariant

STEP D

$$D^{(1)} = \frac{B}{\sigma^{(1)}} = \frac{8250}{30000} = \underline{.275}$$

$D^{(2)} = \underline{.220}$ $\quad$ $D^{(3)} = \underline{.183}$

STEP E

Constant stress lines represented by $F'^{(i)} \equiv \dfrac{D^{(i)}}{2\psi_s{}^2\psi_R(1+\psi_R)\sin\beta\cos\beta}$ are plotted in Figure 10. For this calculation, $\psi_s = .974$ = Constant, and $\psi_R = \psi_R(\beta, M_{w_4}) = \psi_R(\beta, 1.45)$ is assumed. The total rotor losses are

esimated following step (B-3) to be

$$(Y_T)_R = (Y_{sec} + Y_K)_R + (Y_P)_R = \underline{.72 \sin^2\beta + .12}$$

The velocity coefficient, ψ_R, is then easily calculated, as in Step (B-3) as a function of variable β with $M_{w_4} = 1.45$. A simple working plot of $\psi_R = \psi_R(\beta)$ constructed from Table I-d is a convenience in Steps (E) through (H).

STEP F

Curves of $F''(\beta)$ for δ = constant are plotted in Figure 10. The range $.52 < \delta < .76$ represents practical limits of interest and increments of .02 are satisfactory.

STEPS G AND H

From intersections of δ = constant and $\bar{\sigma}$ = constant curves of Figure 10, Equation (III-4-15) was solved for η. Plots of $\eta(\beta)_{\bar{\sigma} = \text{const.}}$ are shown for the selected stresses in Figure 11. While not expected to be quantitatively precise, Figure 11 condenses the design variables into an easily digested presentation. Since η, M_{w_3}, R, U, h_4 depend only on θ, δ , β, the selection of a design point to fulfill a specified mission is considerably simplified.

In the present case, one can write,

(Eq. II-4-16), $\quad M_{w_2} \approx 1.675 \ \frac{\delta}{.732} = \underline{2.29\ \delta}$

(Eq. III-4-4), $\quad \theta = \theta\ (\delta, \beta)$, plotted for convenience in the regime of interest.

(Eq. III-4-17), $\quad R \approx 14.1 \ \frac{\theta}{.308} = \underline{45.8\ \theta}$

(Eq. III-4-17), $U \approx 1848 \frac{\theta}{.308} = \underline{6000\,\theta}$

(Eq. III-4-18), $m \approx 1.53\ (45.8\,\theta)^2 = \underline{3220\,\theta^2,\ \text{lb.}}$

(Eq. III-4-19), $h_4 \approx \frac{.308}{\theta} \frac{\delta}{32600} \times 1.207 = \underline{1.14 \times 10^{-5}\ \frac{\sigma}{\theta}}$

STEP I

A working stress must be selected. The blade temperatures may be estimated, for a (turbulent) recovery factor of about .9, to be,

$$T_{blade} \leq T_2 + .9 \frac{W_2^2}{2gJC_P} = 1328 + .9 \times \frac{4390^2}{4.13 \times 10^4} = \underline{1747^\circ R = 1287^\circ F.}$$

From Figure 11, one notes that efficiencies are reasonably good for $\bar{\sigma} = 37500$, with relatively little gain to be achieved at higher stresses. Experience would indicate $\bar{\sigma} = 37500$ to be a logical choice for a rocket turbine application of short running time. Ample safety factor should be available for a blade material such as Inconel 703C at this temperature.

In Figure 11 for $\bar{\sigma} = 37500$, the regime, $.60 \leq \delta \leq .68$ appears most practical. A rough idea of the trade-off between fuel consumption and turbine weight may be quickly made if desired. For example, comparing points at $\delta_1 = .66$ and $\delta_2 = .62$ shows the latter turbine would weigh approximately $\Delta m = 3220(\theta_1^2 - \theta_2^2) = 3220(.42^2 - .37^2) = \underline{127\ \text{lb. more.}}$ The corresponding reduction in fuel consumption would be

$$\Delta\dot{W} = \dot{W}_2 - \dot{W}_1 = \frac{550/778\ SHP}{\Delta H_{is}} \left(\frac{1}{\eta_1} - \frac{1}{\eta_2}\right) = \frac{.707 \times 28800}{760} \left(\frac{1}{.764} - \frac{1}{.794}\right) =$$

$$\underline{1.34\ \text{lb/sec.}}$$

The choice of $\delta = .62$ would appear advantageous only if the burning time exceeds

$$\frac{\Delta m}{\Delta \dot{W}_o} = \frac{127}{1.34} = 95 \text{ sec},$$

provided the objective is simply minimizing the sum of turbine weight and total fuel consumed.

In the light of foregoing considerations a choice was made, selecting: $\delta \equiv .64$, $\beta \equiv 60^\circ$ with the assurance $\sigma \approx 37500$. From Figure 11 and Step H, the additional estimates are immediately available:

$$\theta \approx .395$$

$$\eta \approx .78$$

$$\dot{W}_o \approx 34 \text{ lb/sec}$$

$$M_{w_2} \approx 1.46$$

$$R \approx 18.1"$$

$$h_4 \approx 1.08"$$

$$U \approx 2370 \text{ ft/sec}$$

$$m \approx 500 \text{ lb.}$$

The design point selection technique has allowed a logical and systematic choice of operating design point. It appears that a considerable improvement over the original arbitrary choice has been achieved. However, detailed design calculations must follow to verify the choice and remove the inherent approximations.

3. Detailed Design Point Calculations

The absolute gas angle required is

$$\alpha_2 = \cos^{-1}(\delta \cos \beta_2) = \cos^{-1}(.64 \cos 60^\circ) = \underline{71.35^\circ}$$

and $\theta = 1.0 \sin \alpha_2 - \delta \cos \beta_2 = \sin 71.35^\circ - .64 \sin 60^\circ = \underline{.392}$

(a) Recalculation of stator velocity coefficient, ψ_s

In the manner of Step (B-1), ψ_s must be changed to incorporate the revised α_2 and nozzle height. For an estimated $\psi_s \approx .96$,

$$T_2 \approx 2200 - .96^2 \frac{760}{.827} = \underline{1355^\circ R}$$

$$h_2 = \frac{34 \times 128.8 \times 1355}{30\ (.96 \times 6160 \cos 71.35^\circ)\ 2\pi \times 18.1} = .92", \text{ approximate}$$

annulus height. For $\alpha_m \equiv \tan^{-1}(\frac{1}{2} \tan 71.35^\circ) = 55.9^\circ$.

$$(Y_{sec})_s = \frac{.13}{.92} \frac{\sin^2 71.35^\circ}{\cos 55.9^\circ} = \underline{.224} \qquad (Y_P)_s \approx \underline{.06}$$

Total stator losses, $(Y_{tot})_s = .28$. For $M_2 \approx 2.2$, Table I-d gives $\psi_s = \underline{\underline{.965}}$.

It is evident that both $(C_P)_s$ and ψ_s depend on the, as yet unknown, value of M_2 - estimated to be 2.2. In subsequent calculations it is assumed $\psi_s \equiv .965$ to determine the actual M_2. The value of C_P will then be revised, where necessary, to coincide with the newly calculated M_2.

(b) Determination of some velocity triangle components

$V_2 = .965 \times 6160 = \underline{5950 \text{ ft/sec}}$

$W_2 = \delta V_2 = .64 \times 5950 = \underline{3810}$

$\frac{U}{C_o} = \frac{2330}{6160} = \underline{.378}$

$a_2 = 72.0 \sqrt{1345} = \underline{2640}$

$M_{w_2} = \frac{3810}{2640} = \underline{1.44}$

$V_{ax,2} = 5950 \cos 71.35^\circ = \underline{1900}$

$U = \psi_s C_o \theta = 5950 \times .392 = \underline{2330}$

$T_2 = 2200 - .965^2 \frac{760}{.827} = \underline{1345^\circ R}$

$M_2 = \frac{V_2}{a_2} = \frac{5950}{2640} = \underline{2.25}$

Estimate $M_{w_4} = \dfrac{\psi_R W_2}{72.0\sqrt{T_4}} \approx \dfrac{.91 \times 3810}{72.0\sqrt{1413}} = \underline{1.28}$, with $T_4 \approx 1413$ (Step B-5)

(c) Determination of rotor velocity coefficient, ψ_R

$(Y_{sec})_R = .48 \sin^2 60^\circ = \underline{.36}$ $\quad$ $(Y_k)_R = 8 \times .03 \sin^2 60^\circ = \underline{.18}$

$(Y_P)_R \approx \underline{.12}$, $\quad$ and estimated $\quad$ $(Y_T)_R = \underline{.66}$

From Table I-d, for $M_{w_4} = 1.28$, $\psi_R = \underline{.871}$.

An estimated $\psi_R = .881$ is obtained for comparison from the subsonic reference curve of Figure 6.

(d) Completion of velocity triangle and performance calculations

$W_4 = .871 \times 3810 = \underline{3320 \text{ ft/sec}}$ $\quad$ $V_{ax,4} = \psi_R V_{ax,2} = .871 \times 1900 = \underline{1655}$

$V_4 = \sqrt{1655^2 + (3320 \cos 60^\circ - 2330)^2} = \underline{1740}$ $\quad$ $\alpha = \cos^{-1}\left(\dfrac{1655}{1740}\right) = \underline{18.2^\circ}$

mean radius, $R = \dfrac{60 \times 2330}{2\pi \times 15000} \times 12 = \underline{17.8"}$

Work output, $W = \dfrac{2330 \times 3810 \times 1.871 \sin 60^\circ}{2.5 \times 10^4} = 575$ Btu/lb.

$\eta = \dfrac{W}{\Delta H_{IS}} = \dfrac{575}{760} = \underline{.756}$ $\quad$ $\overset{\circ}{W} = \dfrac{.707 \times 28800}{575} = \underline{35.4 \text{ lb/sec}}$

The calculated efficiency appears reasonable but perhaps slightly optimistic, compared with Figure 1.

(e) Temperatures and total head efficiency

$T_4 = T_2 + \dfrac{W_2^2}{2gJC_P}(1 - \psi_R^2) = 1345 + \dfrac{3810^2}{4.13 \times 10^4} \times .241 = \underline{1429^\circ R}$

$T_4' = T_4 + \dfrac{V_4^2}{2gJC_P} = 1429 + \dfrac{1740^2}{4.13 \times 10^4} = \underline{1502^\circ R}$

$$W = C_P \Delta T' = .827\ (2200 - 1502) = \underline{577\ \text{Btu/lb.}}$$

$$M_{W_4} = \frac{W_4}{72.0\sqrt{T_4}} = \frac{3320}{72.0\sqrt{1429}} = \underline{1.22}$$

$$M_4 = \frac{1740}{72.0\sqrt{T_4}} = \frac{1740}{72.0\sqrt{1429}} = \underline{.64}$$

$$P_4' = P_4 \left(1 + \frac{\gamma-1}{2} M_4^2\right)^{\frac{\gamma}{\gamma-1}} = 30\ (1 + .125 \times .64^2)^{5.0} = \underline{38.5\ \text{psia}}$$

$$\eta_T = \frac{W}{\Delta H'_{IS}} = \frac{575}{.827 \times 2200\ [1 - (\frac{38.5}{450})^{.20}]} = \underline{.815}$$

4. Nozzle Flow Analysis and Profile Layout

A detailed analysis of the stator losses and required geometric layout is necessary. Pertinent assumptions are:

(a) flow within the nozzles (stations 0-1) is considered isentropic,

(b) all stator losses occur in and downstream of the exit plane, between stations 1 and 2, and a uniform flow is established beyond station 2. The losses between 1 and 2 are represented by the coefficient $\psi_s = .965$,

(c) continuity is satisfied between 1 and 2,

(d) tangential momentum is conserved between 1 and 2.

(e) the flow is adiabatic, $T_2' = T_1'$.

The continuity equation is developed analogous to that expressed by Equation (II-6-7) except using total temperatures and pressures. The resulting relation is

$$\cos \alpha_1 = \left(\frac{t}{s}\right)_s + C_P \frac{M_2}{M_1} \left(\frac{1 + .125\ M_1^2}{1 + .125\ M_2^2}\right)^{4.5} \cos \alpha_2$$

From previous calculations, $\alpha_2 = 71.35^\circ$, $M_2 = 2.25$. The pressure coefficient,

$$C_P \equiv \frac{P_2'}{P_o'} = \frac{30\ (1 + .125 \times 2.25^2)^{5.0}}{450} = .773$$

Hence, there is

$$\cos \alpha_1 = \left(\frac{t}{s}\right)_s + .0613\ \frac{(1 + .125\ M_1^2)^{4.5}}{M_1} \qquad (1)$$

Tangential momentum conservation gives $V_1 \sin \alpha_1 = V_2 \sin \alpha_2$.

$$M_1 \sqrt{\gamma g \bar{R} T_1}\ \sin \alpha_1 = M_1 \sqrt{\gamma g \bar{R}}\ \sqrt{\frac{T_1'}{1 + \frac{\gamma-1}{2} M_1^2}}\ \sin \alpha_1 = M_2 \sqrt{\gamma g \bar{R}}\ \sqrt{\frac{T_2'}{1 + \frac{\gamma-1}{2} M_2^2}}\ \sin \alpha_2$$

or

$$\sin \alpha_1 = \frac{M_2}{M_1}\ \sqrt{\frac{1 + \frac{\gamma-1}{2} M_1^2}{1 + \frac{\gamma-1}{2} M_2^2}}\ \sin \alpha_2 = \frac{2.25}{\sqrt{1 + .125 \times 2.25^2}}\ \frac{\sqrt{1 + .125 M_1^2}}{M_1} \sin 71.35^\circ$$

$$\sin \alpha_1 = 1.670\ \frac{\sqrt{1 + .125\ M_1^2}}{M_1} \qquad (2)$$

For a nozzle with no trailing edge thickness, simultaneous solution of (1) and (2) gives $M_1 = 2.150$, $\alpha_1 = 77.2^\circ$.

For structural integrity a nozzle having 10% "blockage," or $t/S \cos \alpha_2 = .10$, is selected. Equation (1) then becomes

$$\cos \alpha_1 = .0682\ \frac{(1 + .125\ M_1^2)^{4.5}}{M_1} \qquad (3)$$

Solution of (2) and (3) gives $\alpha_1 = 75.3^\circ$, $M_1 = 2.178$ for the required nozzle exit conditions consistent with the desired (velocity triangle of Figure 12) discharge flow. The blade angle turns out to be about the largest practically acceptable value. If desired, the magnitude

of α_1 could be decreased by providing a slight annular expansion between stator and rotor.

The type of nozzle profile is probably not critical. A "sharp-corner" nozzle of the type discussed in Reference 16 was chosen somewhat arbitrarily. The sharp-corner nozzle, in general, provides for the shortest possible nozzle length capable of a uniform discharge flow. Its properties become much more favorable in cases having larger nozzle pressure ratios and lower discharge angles than the present example.

Rather than using a full characteristics network, the approximate nozzle contour required was obtained by calculating the required throat angle, over-all area ratio, and the approximate orientation of the limiting characteristics. The angle of turn at the throat is simply $\frac{1}{2}\nu_1$, where $\nu_1 = \nu_1(M_1)$ the Prandtl-Meyer property angle corresponding to the exit.

$$\nu_1 \equiv \sqrt{\frac{\gamma+1}{\gamma-1}}\tan^{-1}\sqrt{\frac{\gamma-1}{\gamma+1}(M_1^2 - 1)} - \tan^{-1}\sqrt{M^2 - 1}$$

and $\frac{1}{2}(\nu_1)_{M_1} = 2.178 = 17.9^\circ$, the required angle. The required area ratio is obtained from one-dimensional flow theory. The relation is, (e.g. Reference 17, problem 4.20),

$$\frac{A_1}{A_t} = \frac{(\frac{P_1'}{P_1})^{\gamma+1/2\gamma}}{\sqrt{(\frac{2}{\gamma-1})\left[(\frac{P_1'}{P_1})^{\gamma-1/\gamma} - 1\right]}} \left(\frac{2}{\gamma+1}\right)^{\gamma+1/2(\gamma-1)} .$$

For $M_1 = 2.178$,

$$P_1'/P_1 = (1 + .125 \times 2.178^2)^{5.0} = 10.22$$

and

$$\frac{A_1}{A_t} = \frac{(10.22)^{.90}}{\sqrt{8\,(10.22^{.20} - 1}} \left(\frac{8}{9}\right)^{4.5} = \underline{2.20} \ .$$

The schematic nozzle layout is shown in Figure 13.

The limiting characteristic of the throat fan, ab, stands at approximately $\phi + \mu = -17.9^\circ + \sin^{-1}\left[\frac{1}{(M)_{\nu=17.9^\circ}}\right] = -17.9^\circ + \sin^{-1}\left(\frac{1}{1.64}\right) = \underline{19.6^\circ}$. The limiting reflected characteristic, bc, stands at approximately $\mu = \sin^{-1}\left(\frac{1}{2.178}\right) = 27.4^\circ$. Thus the minimum nozzle length is

$$\frac{w_t}{\tan 19.6^\circ} + \frac{2.20\ w_t}{\tan 27.4^\circ} = (2.8 + 4.25)\ w_t = \underline{7.05\ w_t}$$

However, due to the required truncation of the nozzle at $\frac{\pi}{2} - \alpha_1 = 14.7^\circ$, the dimension bg must be no less than $\frac{2.20\ w_t}{\tan 14.7^\circ} = 8.38\ w_t$. Hence, minimum throat to discharge dimension, parallel to nozzle axis, is eb + bg = $2.8 + 8.4\ w_t = \underline{11.2\ w_t}$. The resulting nozzle profile layout is shown in Figure 14a.

Since the edge thickness, t, is 1/10 the total width, $t = 1/9 \times 2.20\ w_t = .244\ w_t$. Total width is $w = 2.444\ w_t$. The spacing between blades is $s = \frac{w}{\cos \alpha_1} = \frac{2.444\ w_t}{\cos 75.3^\circ} = \underline{9.65\ w_t}$. The number of blades $Z_s = \frac{2\pi R}{s} = \frac{2\pi \times 17.8}{9.65\ w_t} = \frac{11.59}{w_t}$. For a selected throat dimension $\underline{\underline{w_t = .290",\ Z_s = 40 \text{ blades.}}}$ The nozzle cascade is illustrated in Figure 14b.

The height of the nozzles (and annulus), may be more precisely calculated,

$$h_2 = \frac{\overset{\circ}{W}\,\bar{R}\,T_2}{P_2 V_{ax,2}\,2\pi R} = \frac{35.4 \times 128.8 \times 1345}{30 \times 1900 \times 2\pi \times 17.8} = \underline{\underline{.961" = h_1}}$$

The total throat area is $Z_s h w_t = 40 \times .961 \times .290 = \underline{\underline{11.14\ in^2}}$.

With the nozzle dimensions fully determined, the calculated stator coefficient of III(a) should be checked. For a thickness ratio $\tau/c = .21$ and solidity $c/s = 1.44$, Figure 2a and Equation II-2-1 gives $(Y_P)_s = \frac{.21}{.20} \times .05 = .053$. The secondary losses are $(Y_{sec})_s = \frac{.13}{.961} \frac{\sin^2 75.3^\circ}{\cos 62.3^\circ} = .272$, where the blade angle rather than the gas angle is employed to provide the most conservative estimate. Total losses $(Y_{tot})_s = .33$ exceed the estimated .28 of previous calculations. Hence, from Table I-d, the estimated $\psi_s = .965$ may be about .004 too optimistic, but recalculation of IV-3 seems unnecessary.

5. Rotor Flow Analysis and Profile Layout

A leading edge thickness ratio, t/s, must be selected first so that incidence may be determined. For a chord of about 1", an expected solidity $c/s \approx 2.5$, and a desired edge thickness of about .020", there is $t/s = t/c \cdot c/s \approx .020 \times 2.5 = .050$.

The incidence, $\beta_2 - \beta_3$, may be determined from Equation (II-6-10), $\cos \beta_3 = \frac{t}{s} + \frac{\cos \beta_2}{C_P}$. From considerations discussed in II-6, it is assumed that about one-quarter of the rotor losses occur around the leading edge - between stations 2 and 3.

For $(Y_{LE})_R = \frac{1}{4} (Y_T)_R = \frac{.66}{4} = .165$ there results from Table I-c, $(C_P)_{LE} = C_P(M = 1.44, Y = .165) = \underline{.90}$

Hence $\beta_3 = \cos^{-1} (.050 + \frac{\cos 60^\circ}{.90}) = \underline{52.8^\circ}$ and the incidence is 7.2°. The assumed pressure loss has increased the incidence by about 3.7° from the isentropic case. It is of interest that, were the blade angle, β_3, equal to 60°, the relative incident gas angle would be about 66.1° and the nozzle pressure ratio would be greatly reduced from the desired 15 to 1 value.

The rotor profile was laid out following the scheme of Reference 13 as summarized in Section II-5 of the present report. As discussed in Section II-6, the rotor entrance Mach number, M_{w_3}, is assumed equal to $M_{w_2} = 1.44$. It may exceed this value slightly, as suggested by the discussion of II-6.

By Equation II-5-1,

$$\left(\frac{r_i}{r_{out}}\right)_{tran} \geq \cos \mu_3 = \cos\left(\sin^{-1} \frac{1}{M_{w_3}}\right)$$

$$\left(\frac{r_i}{r_{out}}\right)_{tran} \geq \cos\left(\sin^{-1} \frac{1}{1.44}\right) = .720$$

$$\left(\frac{w}{r_M}\right)_{tran} \equiv \frac{r_{out} - r_i}{\frac{r_{out} + r_i}{2}} \leq \frac{2(1 - .720)}{1 + .720} = .326$$

Theoretically a channel width-to-radius ratio of .326 would just insure tangency of Mach waves with the convex surface, while allowing an excessively large Prandtl-Meyer acceleration on this surface. Hence, the authors recommend at least a 20 to 30% reduction in $\left(\frac{w}{r_M}\right)_{tran}$. Accordingly, a design value, $\left(\frac{w}{r_M}\right)_{tran} \equiv .22$ was selected. For an arbitrary construction scale, let $(r_M)_{tran} = 1.0$, $w_{tran} = w_{cen} = .22$, $(r_o)_{tran} = 1.11$, $(r_i)_{tran} = .89$. Since the curvature is to be doubled in the central section, $(r_M)_{cen} = .50$, $(r_{out})_{cen} = .61$, $(r_i)_{cen} = .39$.

The profile is constructed, to arbitrary scale of 1.10" channel width, in Figure 15. The transition curvature is 15° and the leading edge consists of a 10° wedge. This is slightly less than the maximum angle consistent with an attached shock. The edges could probably be rounded at a slight sacrifice in performance. From construction,

the solidity, $c/s = 2.88$ and the thickness ratio $\tau/c = .160$. For a selected chord of 1", thickness at the shoulder chamber is approximately .020" and the scale of Figure 15 is 5.74/1.

The number of blades required is calculated from

$$Z_R = \frac{2\pi R}{s} = \frac{2\pi R}{\frac{s}{c} \cdot c} = \frac{2\pi \times 17.8}{\frac{1}{2.88}} = \underline{322 \text{ blades}}$$

The rotor losses may be recalculated more precisely for comparison with $(Y_T)_R = .66$ obtained in IV-3. For $\tau/c = .16$ and $s/c = .35$, Figure 2b and Equation (II-2-1) gives $(Y_P)_R = \frac{.16}{.20} \times .13 = .104$. The revised best estimate of rotor loss is $(Y_T)_R = .64$. From Table I-d,

$$\psi_R = \psi_R(Y = .64,\ M = 1.22) = .868 ,$$

compared to the previous estimate of .871. From Equation (III-2-3), for the final estimates of ψ_s, ψ_R, the final efficiency estimate is $\underline{\eta = .748}$. From IV-4, $h_2 = h_3 = .961$", and

$$h_4 = h_2 \frac{T_4}{T_2} \frac{1}{\psi_R} = .961 \frac{1429}{1345} \times \frac{1}{.868} = \underline{1.172"}$$

From IV-2, $\sigma = 1910\, Rh_4 = 1910 \times 17.8 \times 1.172 = \underline{39800 \text{ psi}}$

$$B \equiv \sigma\eta\psi_R \delta \cos\beta = 39800 \times .748 \times .868 \times .64 \cos 60^\circ = \underline{8270}$$

Total weight, $m = 3220\, \lambda^2 = 3220\, (.392)^2 = \underline{495 \text{ lb.}}$

6. Discussion of Resulting Design

The major numerical results are compiled for comparison with estimates of IV-2.

η	=	.748	B	=	8270 psi
$\dot{W}_o$	=	35.4 lb/sec.	β	=	60^o
σ	=	39800 psi	M_{w_2}	=	1.44
R	=	17.8"	M_{w_4}	=	1.22
ψ_s	=	.961	θ	=	.392
ψ_R	=	.868	δ	=	.64

The calculated efficiency of .748 agrees well with that indicated in Figure 1 for U/C_o = .378. Hence, a confident prediction of efficiencies well above .7 offers encouragement for improvement over the previously demonstrated performances of supersonic turbines.

The Design Point Selection Technique, leading to Figure 11, proves to be of great assistance in presenting a thumbnail sketch of available design choices. The slight variation from the predicted values of IV-2 was obviously due to the reductions in both ψ_R and ψ_s from the approximations assumed. Of particular interest is the observation that the "invariant" B changed only .24% from the value based on the original arbitrary design point.

Perhaps the most questionable area of the problem was that of estimating rotor incidence. The theoretical basis is certainly open to speculation, as discussed in II-6.

V. CONCLUSIONS AND DISCUSSION

This investigation indicates that well designed supersonic-rotor single-stage impulse turbines are capable of rather impressive performance. These machines appear to be an attractive compromise between simplicity and high efficiency. Utilizing recent test results, an effort is made to better understand the losses and flow peculiarities of supersonic stages. Many questions are encountered which cannot be decisively resolved without more tests of the quality previously reported by the Aeronautical Research Council of Great Britain.

Analysis of supersonic turbine tests indicate that no appreciable losses need be attributed solely to Mach number effects, provided certain design criteria are followed. The major rotor blade design objective is the prevention of shock-induced flow separation. Profiles have been recently developed by the Aeronautical Research Council which virtually eliminate separation. In supersonic flow these blades have much lower profile losses than the conventional constant-curvature blades commonly used in subsonic rotors. Carefully designed profiles yield considerably greater improvements in total efficiency than in static efficiency. Properly chosen rotor blade flare, accurately reflecting actual losses, has a considerable effect on static efficiency.

Since Mach number level need have no direct effect on blade losses, an extension of the Ainley-Mathieson loss prediction procedures to the supersonic case is proposed. Some straightforward modifications to the basic procedure are adopted. The extension to supersonic flow appears tentatively justified by the meager amount of available test results.

The existence of a unique rotor incidence, in supersonic flow through blades of finite edge thickness, profoundly influences pressure and velocity distributions throughout the stage. The incidence results from continuity requirements which demand a turning, and probably an increase in velocity, at the rotor entrance. The explanation of the phenomenon presented in Reference 14 and based on Prandtl-Meyer corner flow is shown to be unsatisfactory. An alterative explanation is developed based on the assumption of negligible velocity increase. More experimental work is required to yield a clear understanding of this important phenomenon.

A technique is developed to assist the designer in selecting the "optimum" design point for a single-stage impulse turbine having specified RPM, power, and blade root stress. This method is independent of Mach number level and the method of estimating blade losses. It greatly simplifies the decision by promptly resolving design point selection criteria into a readily digested form.

The preliminary design of a large rocket-turbine is developed as a numerical illustration of the foregoing procedures. Blade speeds, but not necessarily stresses, are typically very high in order to reduce leaving losses. The results indicate static efficiencies exceeding .7 may reasonably be anticipated from well designed turbines of this type.

VI. REFERENCES

1. Ainley, D. G., and Mathieson, G. C. R. An Examination of the Flow and Pressure Losses in Blade Rows of Axial-Flow Turbines. A.R.C. R. and M. 2891, 1955.

2. Johnston, I. H., and Dransfield, D. C. The Test Performance of Highly Loaded Turbine Stages Designed for High Pressure Ratio. A.R.C. R. and M. 3242, 1962.

3. Moffitt, T. P. Design and Experimental Investigation of a Single-Stage Turbine With a Rotor Entering Relative Mach Number of 2. NACA RM E58F20a, 1958.

4. Stewart, W. L., Whitney, W. J., and Miser, J. W. Use of Effective Momentum Thickness in Describing Turbine Rotor-Blade Losses. NACA RM E56B29, 1956.

5. Stewart, W. L., Wong, R. Y., and Evans, D. G. Design and Experimental Investigation of Transonic Turbine With Slight Negative Reaction Across Rotor Hub. NACA RM E53L29a, 1954.

6. Wong, R. Y., Monroe, D. E., and Wintucky, W. T. Investigation of Effect of Increased Diffusion of Rotor-Blade Suction-Surface Velocity on Performance of Transonic Turbine. NACA RM E54F03, 1954.

7. Whitney, W. J., Monroe, D. E., and Wong, R. Y. Investigation of Transonic Turbine Designed for Zero Diffusion of Suction-Surface Velocity. NACA RM E54F23, 1954.

8. Whitney, W. J., Wong, R. Y., and Monroe, D. E. Investigation of a Transonic Turbine Designed for a Maximum Rotor-Blade Suction-Surface Relative Mach Number of 1.57. NACA RM E54G27, 1954.

9. Wong, R. Y., and Monroe, D. E. Effect of Stator and Rotor Aspect Ratio on Transonic-Turbine Performance. NASA MEMO 2-11-59E, 1959.

10. Miser, J. W., Stewart, W. L., and Wong, R. Y. Effect of a Reduction in Stator Solidity on Performance of a Transonic Turbine. NACA RM E55L09a, 1956.

11. Stewart, W. L. Analytical Investigation of Multistage-Turbine Efficiency Characteristics in Terms of Work and Speed Requirements. NACA RM E57K22b, 1958.

12. Vavra, M. H. Aero-Thermodynamics and Flow in Turbomachines. John Wiley and Sons, New York, 1960.

13. Stratford, B. S., and Sansome, G. E. Theory and Tunnel Tests of Rotor Blades for Supersonic Turbines. A.R.C. R. and M. 3275, 1962.

14. Stratford, B. S., and Sansome, G. E. The Performance of Supersonic Turbine Nozzles. A.R.C. R. and M. 3273, 1962.

15. Stewart, W. L., Evans, D. G., Whitney, W. J. A Method for Determining Design Characteristics for Rocket Turbodrive Applications. NACA RM E57K25a, 1958.

16. Edelman, G. M. The Design, Development, and Testing of Two-Dimensional Sharp-Cornered Supersonic Nozzles. Rep. No. 22, M.I.T., May 1, 1948.

17. Shapiro, A. M. The Dynamics and Thermodynamics of Compressible Fluid Flow, Vol. 1, The Ronald Press Company, New York, 1953.

A P P E N D I C E S

APPENDIX A

NOMENCLATURE

A - area

B - function defined by Equation III-4-11

c - chord

c_p - constant pressure specific heat

C_P - pressure coefficient; ratio of actual to isentropic total pressure

C_o - isentropic jet velocity corresponding to stage pressure ratio

D - function defined by Equation III-4-12

F - force

F' - function defined by Equation III-4-14a

F" - function defined by Equation III-4-14b

g - gravitational constant

H - enthalpy

h - blade or annulus height

$\Delta h/h$ - rotor tip clearance ratio

i - rotor incidence angle

J - mechanical equivalent of heat, 778 Btu/lb.

M - Mach number

m - mass

N - RPM

P - pressure

R - mean blade radius

$\bar{R}$ - gas constant

s - blade spacing

T - temperature

t - blade edge thickness

U - mean blade speed

V - absolute gas velocity

W - gas velocity measured relative to moving rotor

$\dot{W}$ - mass flow rate

$\mathbb{W}$ - specific work

w - channel width

$Y \equiv \dfrac{\text{total inlet pressure - total exit pressure}}{\text{total exit pressure - static exit pressure}}$, Ainley-Mathieson loss parameter.

Z - number of blades

GREEK LETTERS

α - absolute gas angle

β - relative gas angle

γ - ratio of specific heats

$\delta \equiv W_2/V_2$

$\epsilon = \dfrac{M_{w_3} - M_{w_2}}{M_{w_2}}$

$\Theta \equiv U/V_2$

λ - secondary loss acceleration parameter of Figure 3.

ϕ - wall angle

ψ - velocity coefficient; ratio of actual to isentropic velocity

η - efficiency (static)

σ - rotor blade centrifugal root stress

ρ - density

τ - maximum blade thickness

ν - Prandtl-Meyer angle

μ = $\sin^{-1}\left(\frac{1}{M}\right)$, the Mach angle

ω - angular velocity

SUPERSCRIPTS AND SUBSCRIPTS

$( )'$ - total gas properties referenced to absolute gas velocity

$( )''$ - total relative gas properties, refernced to relative gas velocity

$( )_0$ - stator inlet

$( )_1$ - stator exit plane

$( )_2$ - downstream of stator, after mixing

$( )_3$ - just after rotor leading edge

$( )_4$ - downstream of rotor, after mixing

$( )_A$ - profile A of Section II-5

$( )_{AX}$ - axial component

$( )_B$ - profile B of Section II-5

$( )_C$ - cross section

$( )_{cen}$ - central or mid-chord rotor channel

$( )_i$ - inner or convex rotor profile surface

$( )_{IS}$ - isentropic

$( )_K$ - rotor tip loss

$( )_{LE}$ - rotor leading edge

$( )_M$ - mean rotor profile curvature

$( )_m$ - vector mean angle

$( )_{out}$ - outer or concave rotor profile surface

$( )_P$ - profile loss

$( )_R$ - rotor

$( )_S$ - stator

$( )_{sec}$ - secondary loss

$( )_T$ - total loss, or total head efficiency

$( )_t$ - nozzle throat

$( )_{tran}$ - rotor entrance transition channel

$( )_W$ - corresponding to relative velocity

$( )_x$ - upstream, or inlet, position

$( )_y$ - downstream, or exit, position

APPENDIX B

DEVELOPMENT OF EQUATION II-3-1

By reference to a T-S diagram one may easily show (e.g. Appendix B of Ref. 4) that

$$(C_P)_R = \frac{P_4'/P_o'}{P_2'/P_o'(T_4'/T_o')^{\gamma/\gamma-1}} = \frac{P_4'/P_o'}{(C_P)_s\ (T_4'/T_o')^{\gamma/\gamma-1}}$$

T_4'/T_o' may now be expressed in terms of η_T and p_4'/p_o'. With $T_4'_{,IS}$, the temperature corresponding to an isentropic pressure decrease to p_4', there is $T_4'_{,IS} = T_o'(P_4'/P_o')^{(\gamma-1)/\gamma}$ and

$$T_o' = T_4'_{,IS} = T_o'\left[1 - (P_4'/P_o')^{(\gamma-1)/\gamma}\right]$$

Since

$$\eta_T \equiv \frac{T_o' - T_4'}{T_o' - T_4'_{,IS}} = \frac{T_o' - T_4'}{T_o'\left[1 - (P_4'/P_o')^{(\gamma-1)/\gamma}\right]}$$

there is

$$T_4'/T_o' = (1 - \eta_T) + \eta_T\ (P_4'/P_o')^{\gamma-1/\gamma}$$

and finally,

$$(C_P)_R = \frac{P_4'/P_o'}{(C_P)_s\ \left[(1-\eta_T) + \eta_T(P_4'/P_o')^{(\gamma-1)/\gamma}\right]^{\gamma/\gamma-1}}$$

TABLE I-a

GAMMA =1.40

PRESSURE COEFFICIENT AS FUNCTION OF
Y, M. $\gamma = 1.40$

Y \ M	0.6	0.8	1.0	1.2	1.4	1.6	1.8	2.0	2.2	2.4	2.6	2.8	3.0
.00	1.000	1.000	1.000	1.000	1.000	1.000	1.000	1.000	1.000	1.000	1.000	1.000	1.000
.05	.989	.983	.977	.971	.967	.963	.960	.958	.957	.955	.955	.954	.954
.10	.979	.967	.955	.944	.936	.929	.924	.920	.917	.915	.913	.912	.911
.15	.969	.951	.934	.919	.907	.897	.890	.884	.880	.877	.875	.874	.873
.20	.959	.936	.914	.895	.879	.867	.858	.851	.847	.843	.840	.838	.837
.25	.949	.921	.895	.872	.854	.840	.829	.821	.815	.811	.808	.806	.804
.30	.939	.906	.876	.850	.829	.813	.801	.793	.786	.782	.778	.776	.774
.35	.930	.893	.858	.829	.806	.789	.776	.766	.759	.754	.750	.748	.746
.40	.920	.879	.841	.810	.785	.766	.752	.741	.734	.729	.725	.722	.720
.45	.911	.866	.825	.791	.764	.744	.729	.718	.710	.705	.701	.698	.696
.50	.903	.853	.809	.773	.745	.723	.708	.696	.688	.682	.678	.675	.673
.55	.894	.841	.794	.756	.726	.704	.688	.676	.667	.661	.657	.654	.651
.60	.885	.829	.779	.739	.708	.685	.669	.656	.648	.641	.637	.634	.631
.65	.877	.817	.765	.724	.692	.668	.651	.638	.629	.623	.618	.615	.613
.70	.869	.806	.752	.709	.676	.651	.634	.621	.612	.605	.601	.597	.595
.75	.861	.795	.739	.694	.660	.636	.617	.605	.595	.589	.584	.581	.578
.80	.853	.784	.726	.680	.646	.620	.602	.589	.580	.573	.568	.565	.562
.85	.845	.774	.714	.667	.632	.606	.588	.574	.565	.558	.553	.550	.547
.90	.837	.764	.702	.654	.618	.592	.574	.560	.551	.544	.539	.536	.533
.95	.830	.754	.691	.642	.606	.579	.560	.547	.537	.530	.526	.522	.520
1.00	.822	.744	.679	.630	.593	.567	.548	.534	.525	.518	.513	.509	.507
1.05	.815	.735	.669	.618	.581	.555	.536	.522	.512	.506	.501	.497	.495
1.10	.808	.725	.658	.607	.570	.543	.524	.510	.501	.494	.489	.486	.483
1.15	.801	.717	.648	.597	.559	.532	.513	.499	.490	.483	.478	.474	.472
1.20	.794	.708	.639	.586	.549	.521	.502	.489	.479	.472	.467	.464	.461

TABLE I-b

GAMMA =1.40

VELOCITY COEFFICIENT AS FUNCTION OF
Y, M. γ = 1.40

Y \ M	0.6	0.8	1.0	1.2	1.4	1.6	1.8	2.0	2.2	2.4	2.6	2.8	3.0
.00	1.000	1.000	1.000	1.000	1.000	1.000	1.000	1.000	1.000	1.000	1.000	1.000	1.000
.05	.979	.982	.984	.986	.988	.990	.991	.993	.994	.994	.995	.996	.996
.10	.960	.964	.969	.973	.977	.980	.983	.986	.988	.989	.991	.992	.993
.15	.942	.949	.955	.961	.967	.971	.976	.979	.982	.984	.986	.988	.990
.20	.926	.934	.942	.950	.957	.963	.969	.973	.977	.980	.983	.985	.987
.25	.910	.920	.930	.939	.948	.956	.962	.967	.972	.976	.979	.981	.984
.30	.896	.907	.918	.930	.940	.948	.956	.962	.967	.972	.975	.978	.981
.35	.882	.895	.908	.920	.932	.942	.950	.957	.963	.968	.972	.976	.978
.40	.869	.883	.898	.912	.924	.935	.945	.952	.959	.964	.969	.973	.976
.45	.856	.872	.888	.903	.917	.929	.939	.948	.955	.961	.966	.970	.974
.50	.845	.862	.879	.896	.911	.923	.934	.944	.951	.958	.963	.968	.972
.55	.834	.852	.871	.888	.904	.918	.930	.940	.948	.955	.961	.965	.969
.60	.823	.843	.863	.881	.898	.913	.925	.936	.945	.952	.958	.963	.967
.65	.813	.834	.855	.875	.893	.908	.921	.932	.942	.949	.956	.961	.966
.70	.804	.826	.848	.869	.887	.903	.917	.929	.939	.947	.953	.959	.964
.75	.795	.818	.841	.863	.882	.899	.913	.926	.936	.944	.951	.957	.962
.80	.786	.810	.834	.857	.877	.895	.910	.922	.933	.942	.949	.955	.960
.85	.778	.803	.828	.851	.872	.891	.906	.919	.930	.939	.947	.953	.959
.90	.770	.796	.822	.846	.868	.887	.903	.916	.928	.937	.945	.952	.957
.95	.762	.789	.816	.841	.864	.883	.900	.914	.925	.935	.943	.950	.956
1.00	.755	.783	.810	.836	.860	.880	.897	.911	.923	.933	.941	.948	.954
1.05	.748	.776	.805	.832	.856	.876	.894	.908	.921	.931	.940	.947	.953
1.10	.741	.770	.800	.827	.852	.873	.891	.906	.919	.929	.938	.945	.952
1.15	.735	.765	.795	.823	.848	.870	.888	.903	.916	.927	.936	.944	.950
1.20	.728	.759	.790	.819	.845	.867	.885	.901	.914	.925	.935	.943	.949

TABLE I-c

GAMMA =1.25

PRESSURE COEFFICIENT AS FUNCTION OF
Y, M. $\gamma = 1.25$

Y \ M	0.6	0.8	1.0	1.2	1.4	1.6	1.8	2.0	2.2	2.4	2.6	2.8	3.0
.00	1.000	1.000	1.000	1.000	1.000	1.000	1.000	1.000	1.000	1.000	1.000	1.000	1.000
.05	.990	.984	.978	.973	.968	.964	.961	.958	.957	.955	.955	.954	.953
.10	.981	.969	.957	.947	.938	.930	.924	.920	.917	.915	.913	.912	.911
.15	.971	.954	.937	.922	.909	.899	.891	.885	.880	.877	.875	.873	.872
.20	.962	.940	.918	.899	.883	.869	.859	.852	.847	.843	.840	.838	.837
.25	.953	.926	.900	.877	.857	.842	.830	.822	.815	.811	.808	.805	.804
.30	.944	.913	.882	.856	.834	.816	.803	.793	.786	.781	.778	.775	.773
.35	.935	.899	.865	.835	.811	.792	.778	.767	.759	.754	.750	.747	.745
.40	.927	.887	.849	.816	.790	.769	.754	.742	.734	.728	.724	.721	.719
.45	.918	.874	.833	.798	.769	.748	.731	.719	.710	.704	.700	.697	.695
.50	.910	.862	.818	.780	.750	.727	.710	.697	.688	.682	.677	.674	.672
.55	.902	.851	.803	.764	.732	.708	.690	.677	.667	.661	.656	.653	.650
.60	.894	.839	.789	.748	.715	.690	.671	.657	.648	.641	.636	.633	.630
.65	.886	.828	.776	.732	.698	.672	.653	.639	.629	.622	.617	.614	.612
.70	.879	.817	.762	.717	.682	.656	.636	.622	.612	.605	.600	.596	.594
.75	.871	.807	.750	.703	.667	.640	.620	.606	.595	.588	.583	.580	.577
.80	.864	.796	.737	.690	.653	.625	.605	.590	.580	.572	.567	.564	.561
.85	.856	.786	.726	.676	.639	.611	.590	.575	.565	.558	.552	.549	.546
.90	.849	.777	.714	.664	.625	.597	.576	.561	.551	.543	.538	.535	.532
.95	.842	.767	.703	.652	.613	.584	.563	.548	.537	.530	.525	.521	.519
1.00	.835	.758	.692	.640	.600	.571	.550	.535	.525	.517	.512	.508	.506
1.05	.828	.749	.682	.629	.589	.559	.538	.523	.512	.505	.500	.496	.494
1.10	.821	.740	.671	.618	.577	.548	.527	.511	.501	.493	.488	.485	.482
1.15	.815	.731	.661	.607	.566	.537	.515	.500	.490	.482	.477	.473	.471
1.20	.808	.723	.652	.597	.556	.526	.505	.490	.479	.472	.466	.463	.460

TABLE I-d

GAMMA =1.25

VELOCITY COEFFICIENT AS FUNCTION OF
Y, M. $\gamma = 1.25$

Y \ M	0.6	0.8	1.0	1.2	1.4	1.6	1.8	2.0	2.2	2.4	2.6	2.8	3.0
.00	1.000	1.000	1.000	1.000	1.000	1.000	1.000	1.000	1.000	1.000	1.000	1.000	1.000
.05	.979	.981	.983	.985	.987	.989	.990	.992	.993	.994	.995	.995	.996
.10	.959	.963	.967	.971	.975	.978	.981	.984	.986	.988	.989	.991	.992
.15	.941	.946	.952	.958	.964	.969	.973	.977	.980	.983	.985	.987	.988
.20	.924	.931	.939	.946	.953	.960	.965	.970	.974	.977	.980	.983	.985
.25	.908	.916	.926	.935	.943	.951	.958	.964	.968	.973	.976	.979	.982
.30	.893	.903	.914	.924	.934	.943	.951	.958	.963	.968	.972	.976	.978
.35	.879	.890	.902	.914	.926	.936	.944	.952	.958	.964	.968	.972	.976
.40	.865	.878	.892	.905	.917	.929	.938	.947	.954	.960	.965	.969	.973
.45	.853	.867	.882	.896	.910	.922	.933	.942	.949	.956	.962	.966	.970
.50	.841	.856	.872	.888	.902	.916	.927	.937	.945	.952	.958	.963	.968
.55	.829	.846	.863	.880	.896	.910	.922	.932	.941	.949	.955	.961	.965
.60	.819	.836	.854	.872	.889	.904	.917	.928	.938	.946	.952	.958	.963
.65	.808	.827	.846	.865	.883	.898	.912	.924	.934	.943	.950	.956	.961
.70	.799	.818	.838	.858	.877	.893	.908	.920	.931	.940	.947	.953	.959
.75	.789	.810	.831	.852	.871	.888	.903	.916	.927	.937	.944	.951	.957
.80	.780	.802	.824	.846	.866	.884	.899	.913	.924	.934	.942	.949	.955
.85	.772	.794	.817	.840	.861	.879	.895	.909	.921	.931	.940	.947	.953
.90	.763	.787	.811	.834	.856	.875	.892	.906	.918	.929	.937	.945	.951
.95	.756	.780	.805	.829	.851	.871	.888	.903	.916	.926	.935	.943	.949
1.00	.748	.773	.799	.823	.846	.867	.885	.900	.913	.924	.933	.941	.948
1.05	.741	.766	.793	.818	.842	.863	.881	.897	.910	.922	.931	.939	.946
1.10	.734	.760	.787	.814	.838	.859	.878	.894	.908	.919	.929	.938	.945
1.15	.727	.754	.782	.809	.834	.856	.875	.891	.905	.917	.927	.936	.943
1.20	.721	.748	.777	.805	.830	.852	.872	.889	.903	.915	.926	.934	.942

TABLE II

COMPARISON BETWEEN ESTIMATED AND EXPERIMENTALLY DETERMINED LOSS COEFFICIENTS OF TRANSONIC AND SUPERSONIC TURBINE BLADING ROWS

$\gamma \approx 1.4$

Ref.	c/s	h	$\frac{\Delta h}{h}$	τ/c	M_x	M_y	$(\frac{W_x}{W_y})^2$	$\frac{R_{hub}}{R_{tip}}$	λ	β_x	β_y	Y_P	Y_{sec}	Y_K	Y_T	Est. C_P	Exper. C_P	Est. ψ	Exper. ψ
							ROTOR BLADING												
5	2.81	2.1"	.02	.10	.75	1.02	.54	.70	.014	43.2°	39.8°	.060	.098	.070	.23	.900	.892	-	-
6	2.16	2.1	.02	.13	.75	.86	.76	.70	.023	43.2	38.5	.065	.165	.070	.30	.895	.885	-	-
7	2.86	2.1	.02	.08	.75	1.02	.54	.70	.014	43.2	39.8	.055	.098	.070	.22	.902	.908	-	-
8	2.36	2.1	.02	.13	.75	1.02	.54	.70	.014	43.2	39.8	.070	.098	.070	.24	.897	.898	-	-
9	2.86	2.1	.02	.13	.75	1.02	.54	.70	.014	43.2	39.8	.085	.098	.070	.25	.890	.907	-	-
9	2.86	2.1	.02	.13	.75	1.02	.54	.70	.014	43.2	39.8	.085	.098	.070	.25	.890	.900	-	-
2	2.41	0.8	.038	.29	1.61	1.64	1.0	.89	.030	70	70	.164	.424	.254	.84	-	-	.893	.872
							STATOR BLADING												
9	1.41	2.1	-	.07	.31	1.12	.07	.70	.055	0	61.8°	.010	.066	-	.076	-	-	.978	.981
9	1.41	2.1	-	.07	.31	1.12	.07	.70	.055	0	62.1	.010	.066	-	.076	-	-	.978	.984
9	1.41	2.1	-	.07	.31	1.12	.07	.70	.055	0	62.3	.010	.066	-	.076	-	-	.978	.981
10	1.54	2.1	-	.08	.31	1.12	.07	.70	.055	0	62.1	.012	.066	-	.078	-	-	.977	.982
2	1.79	0.8	-	.09	0	2.13	0	.89	.055	0	76	.022	.342	-	.364	-	-	.960	.955

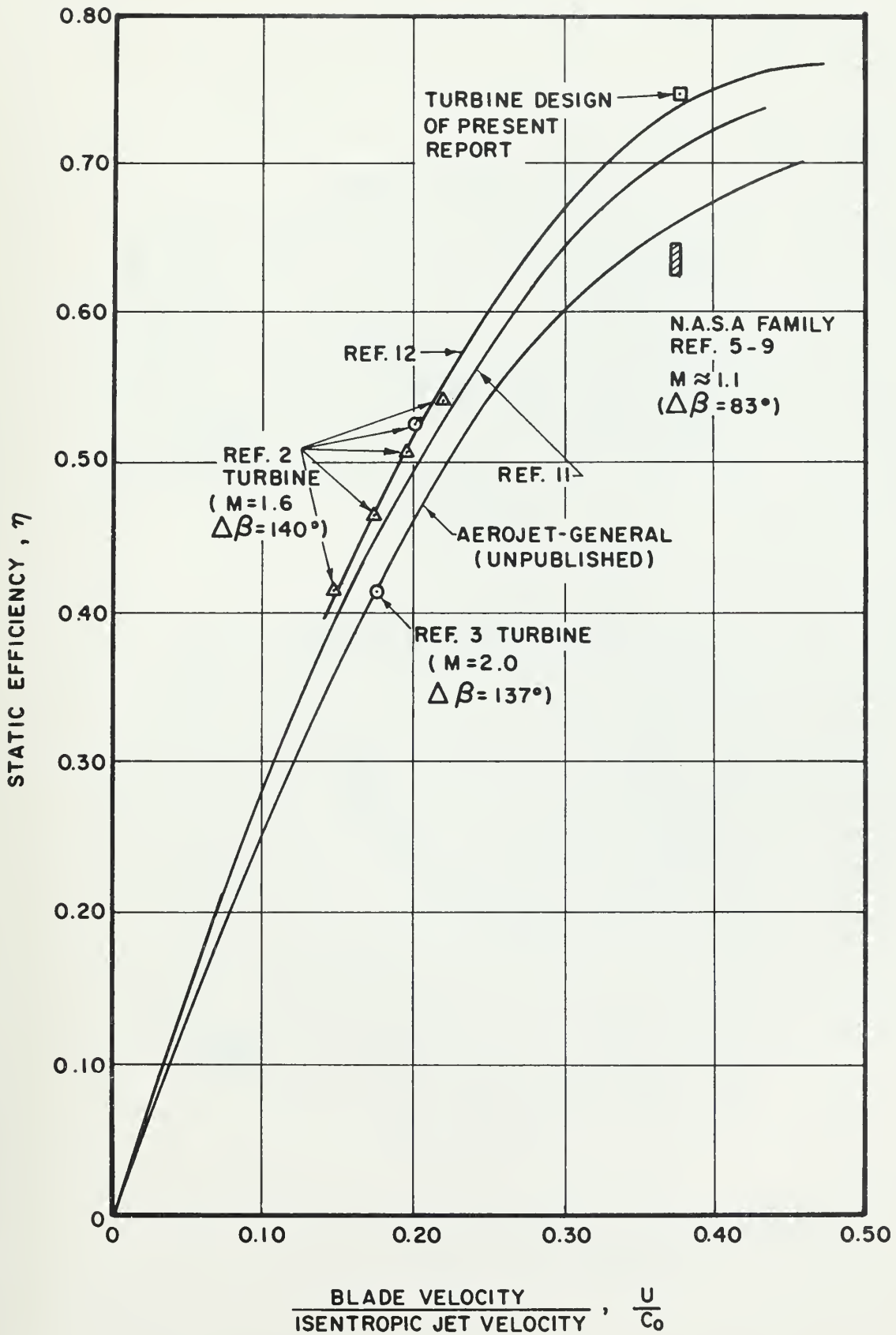

Figure 1. Comparison of Theoretical Efficiency Estimates for (Subsonic) Single Stage Impulse Turbines with Results of Supersonic Turbine Tests.

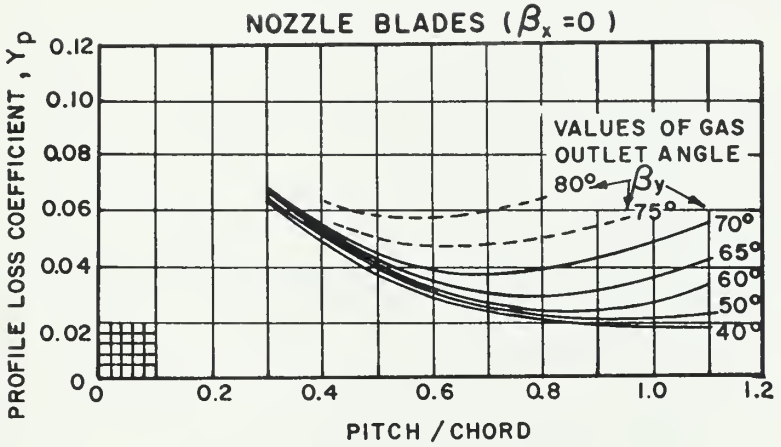

(a)

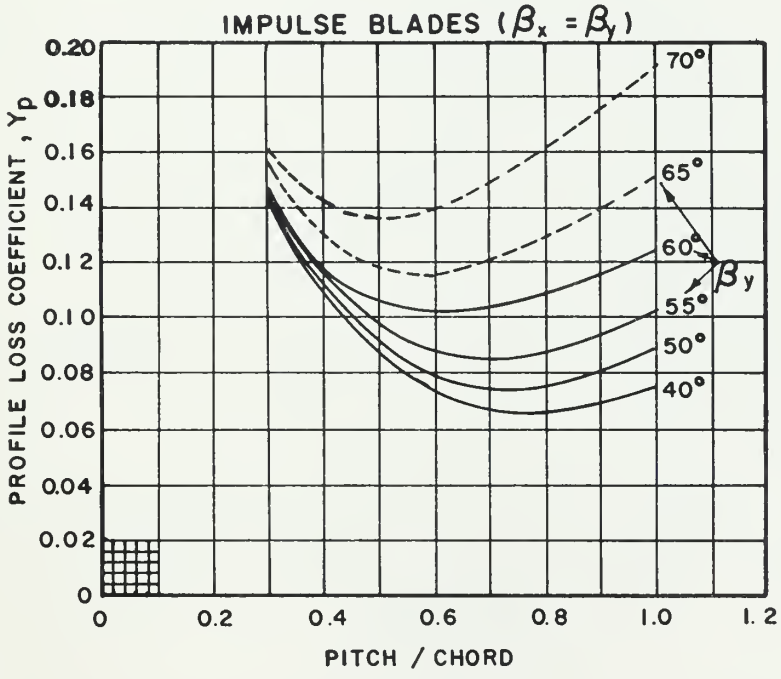

(b)

Figure 2. Profile Loss Coefficients for Conventional Section Blades at Zero Incidence. τ/c = .20; Re = 2 x 10^5; M < 0.6. (From Ref. 1)

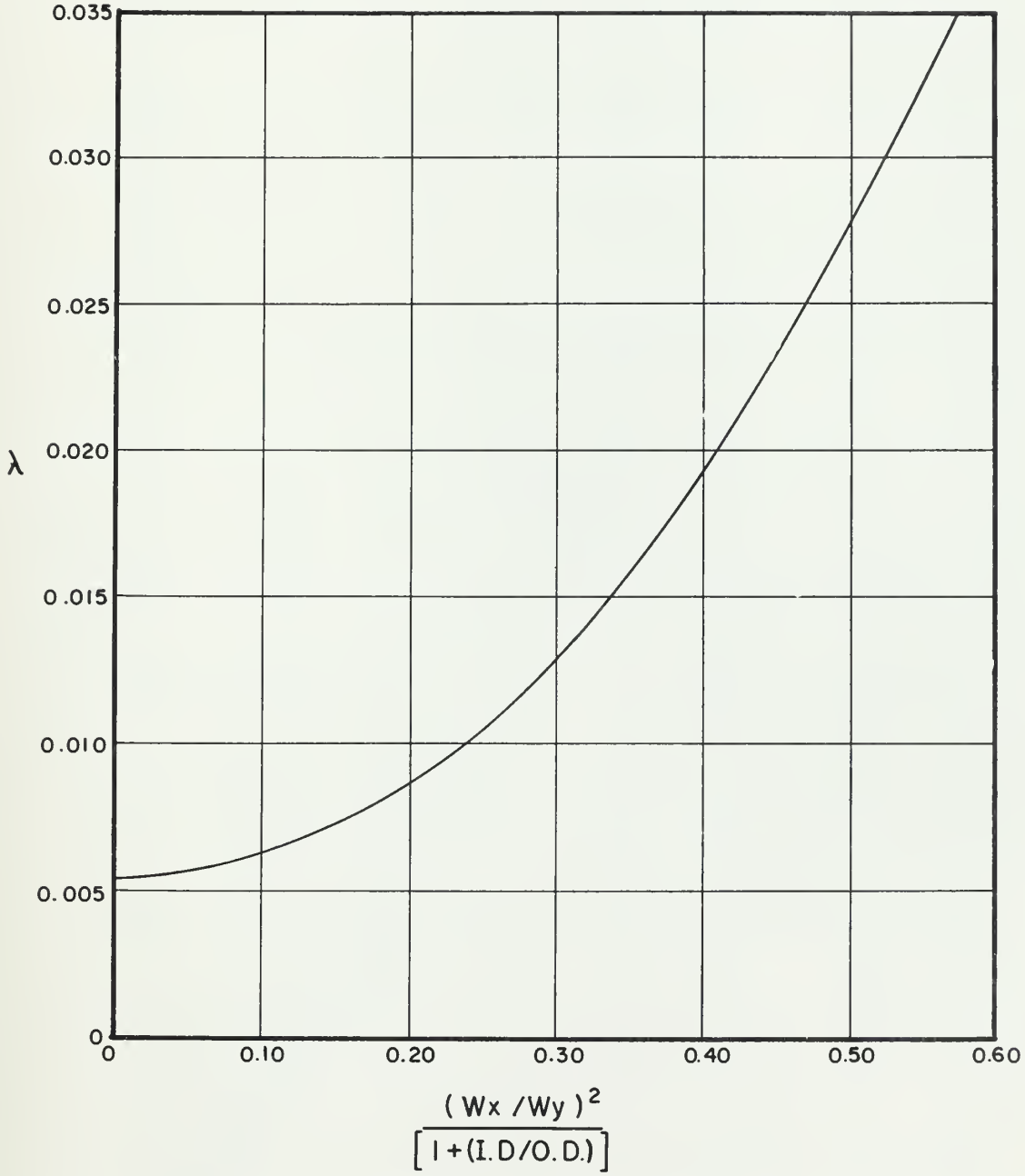

Figure 3. Secondary Loss Acceleration Parameter.

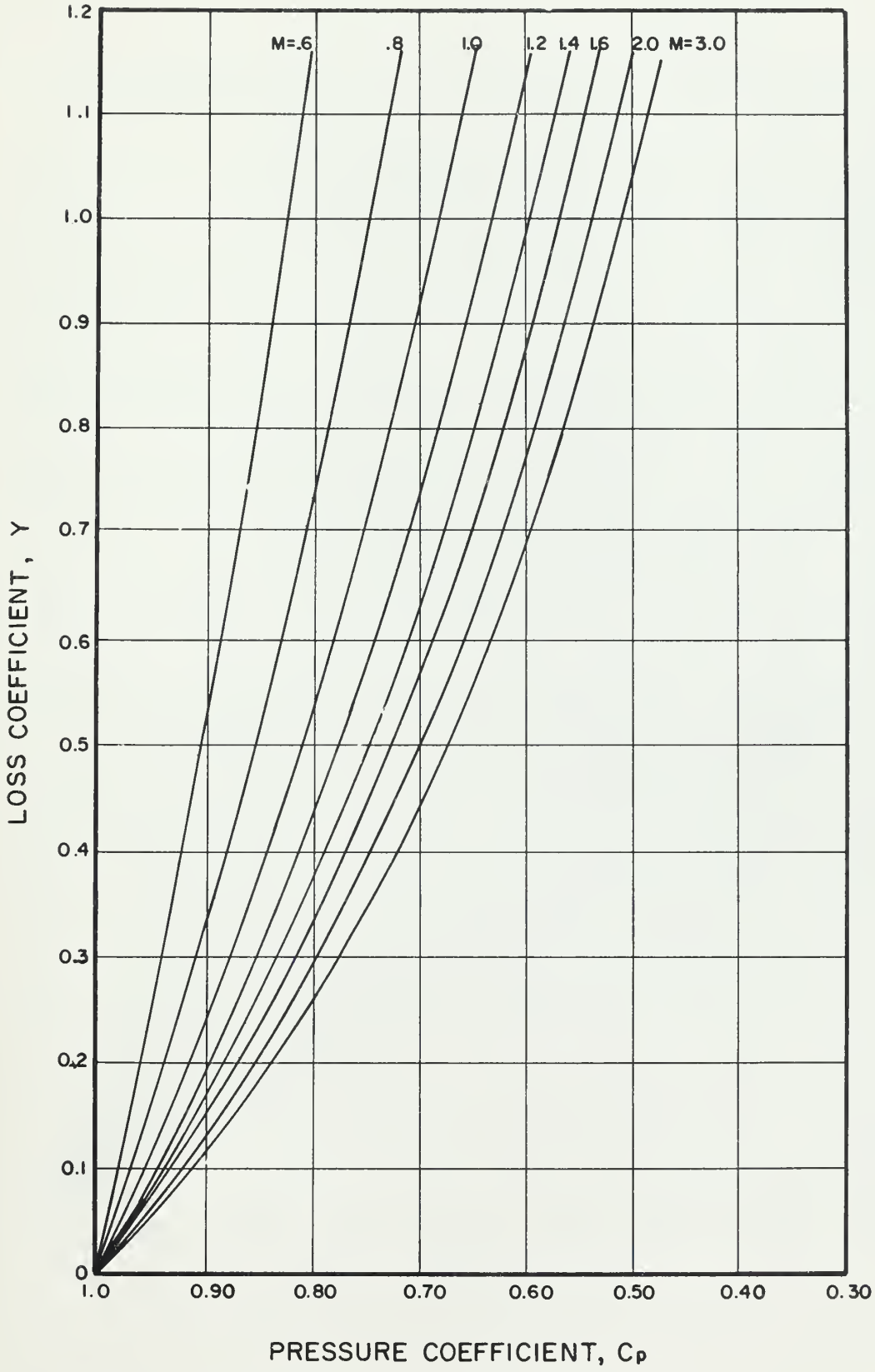

Figure 4. Pressure Coefficient as Function of M, Y, $\gamma = 1.4$.

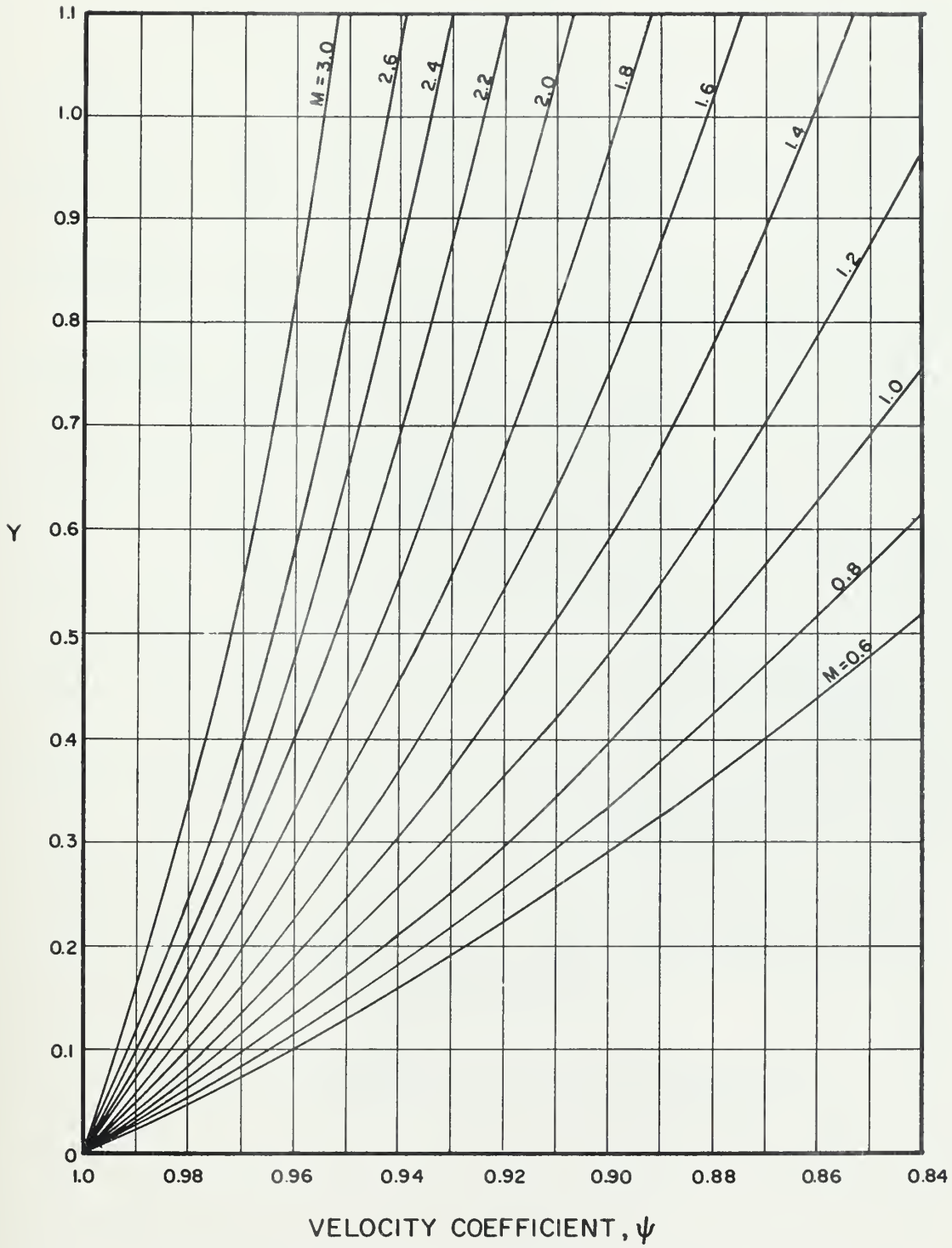

Figure 5. Velocity Coefficient as Function of M, Y, $\gamma = 1.4$.

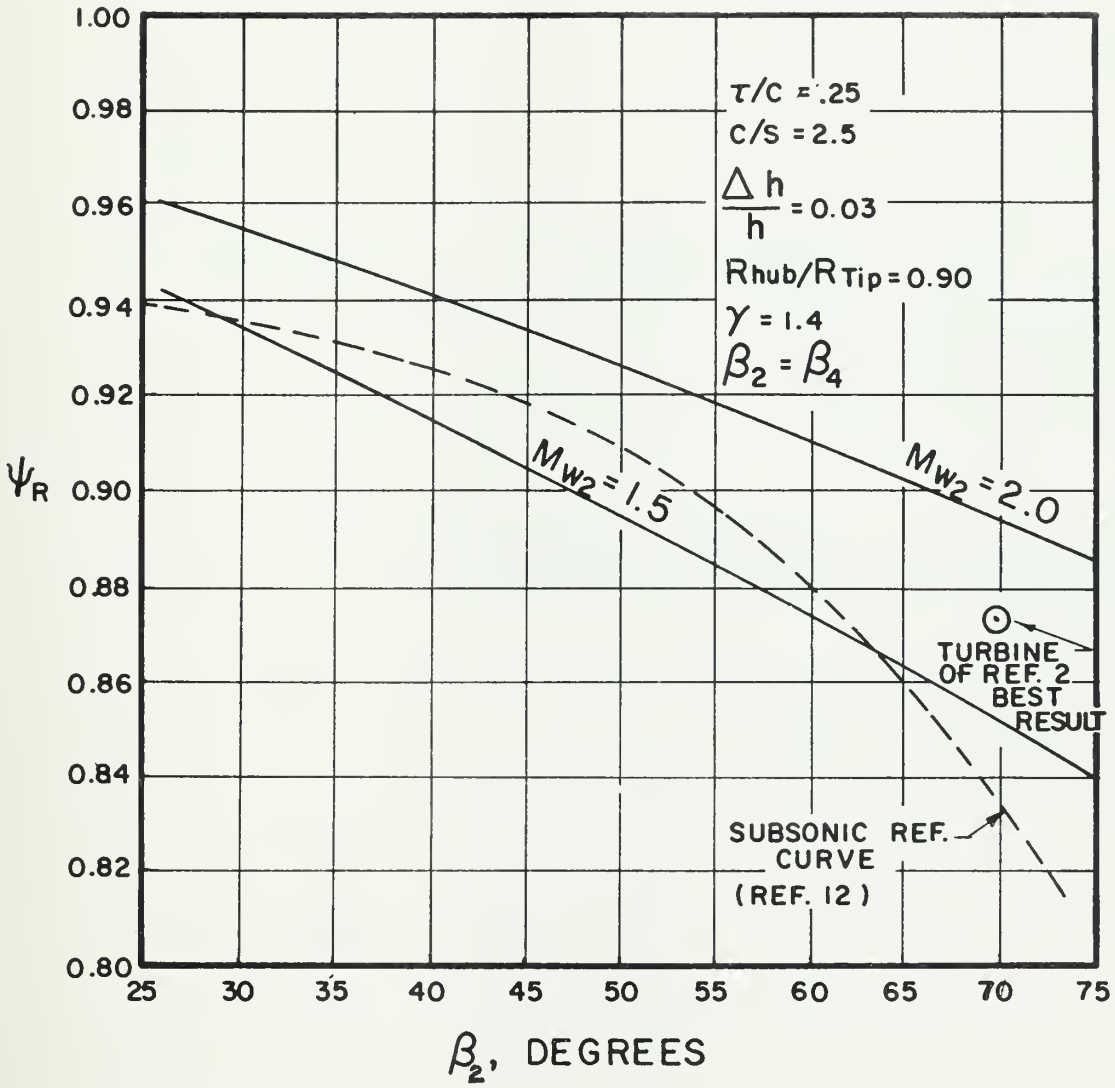

Figure 6. Estimate of Rotor Velocity Coefficient - Typical Impulse Blade in Supersonic Flow.

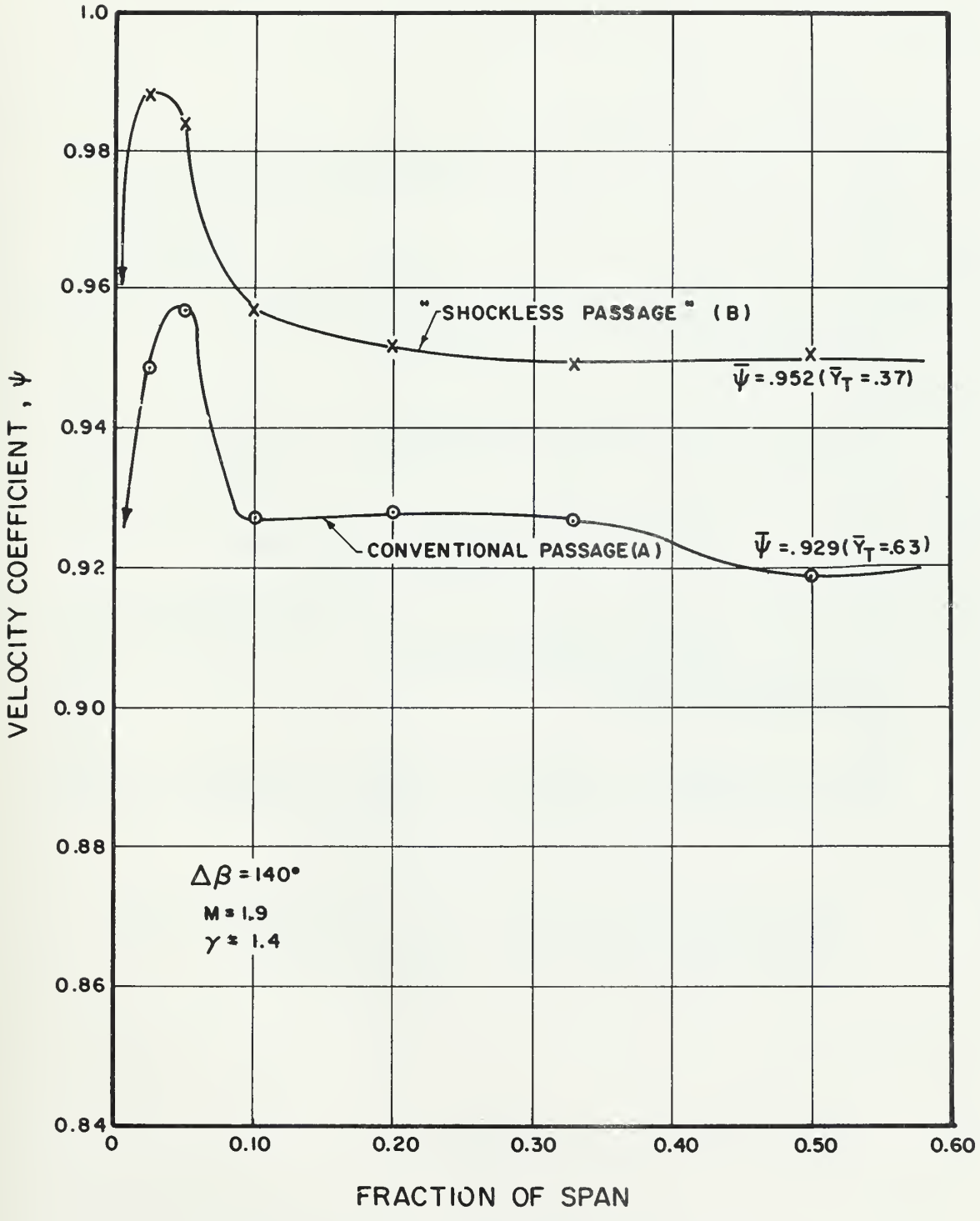

Figure 7. Cascade Loss Results of Reference 13.

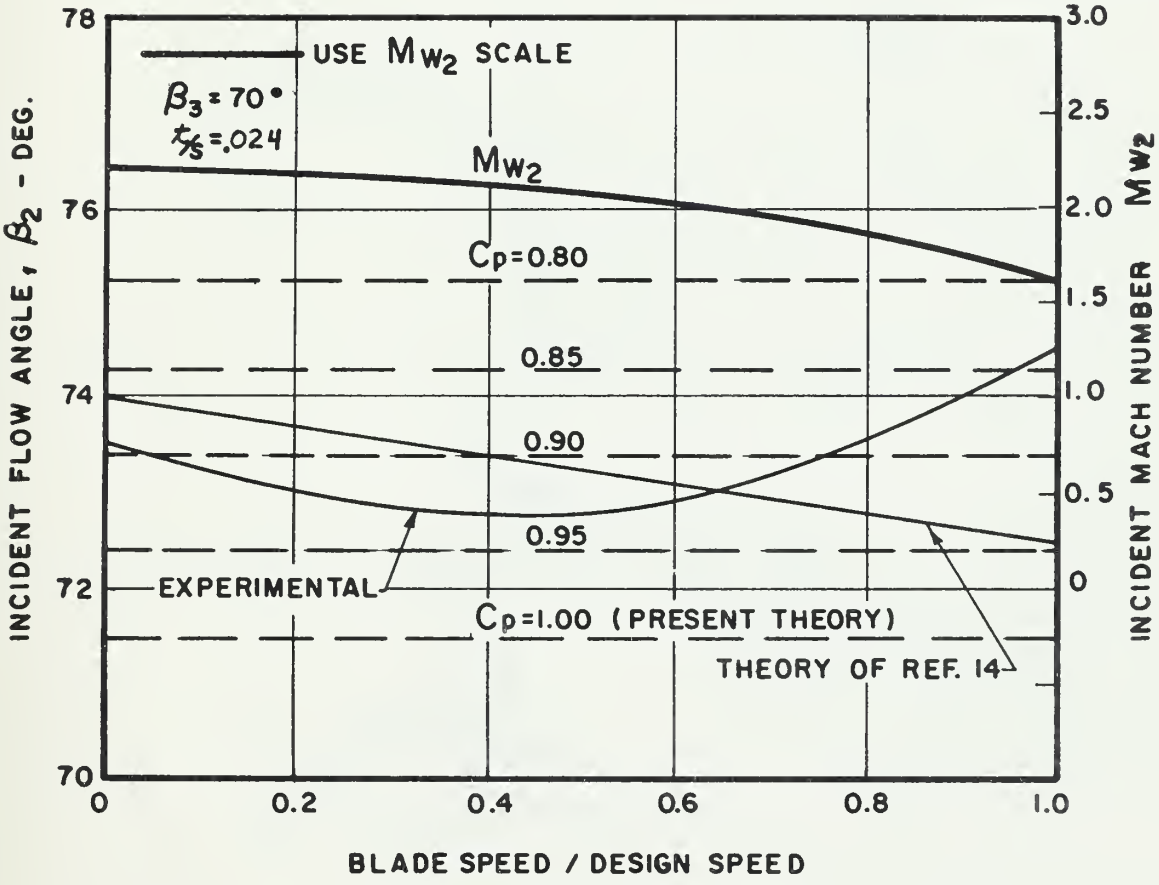

Figure 8. Comparison of Rotor Incidence From Experiment and Two Theories - For Turbine of Reference 2.

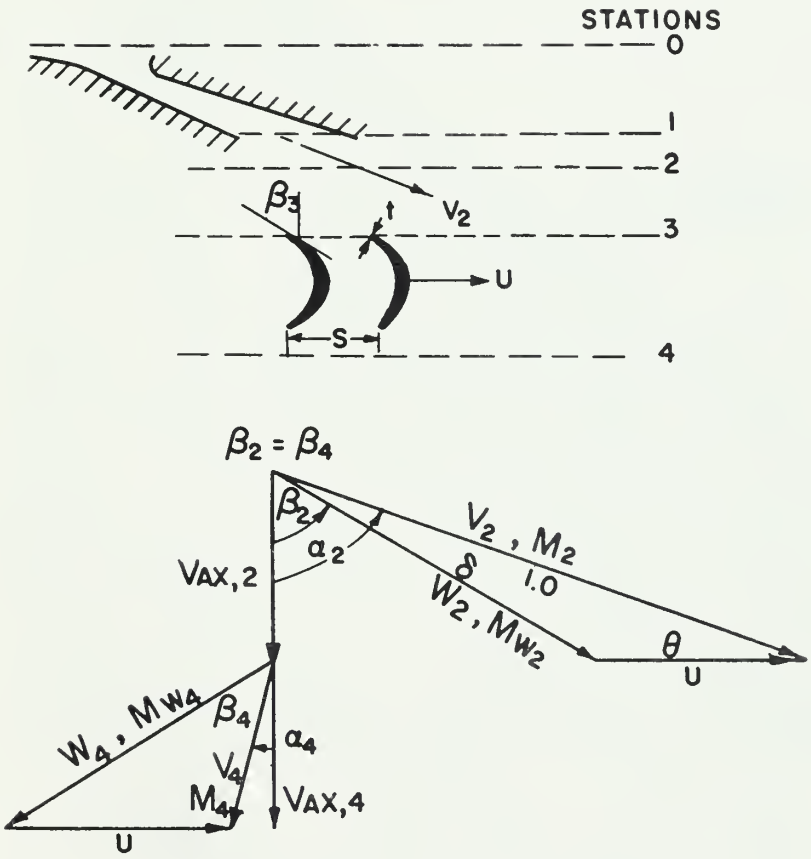

Figure 9. Velocity Triangle Nomenclature.

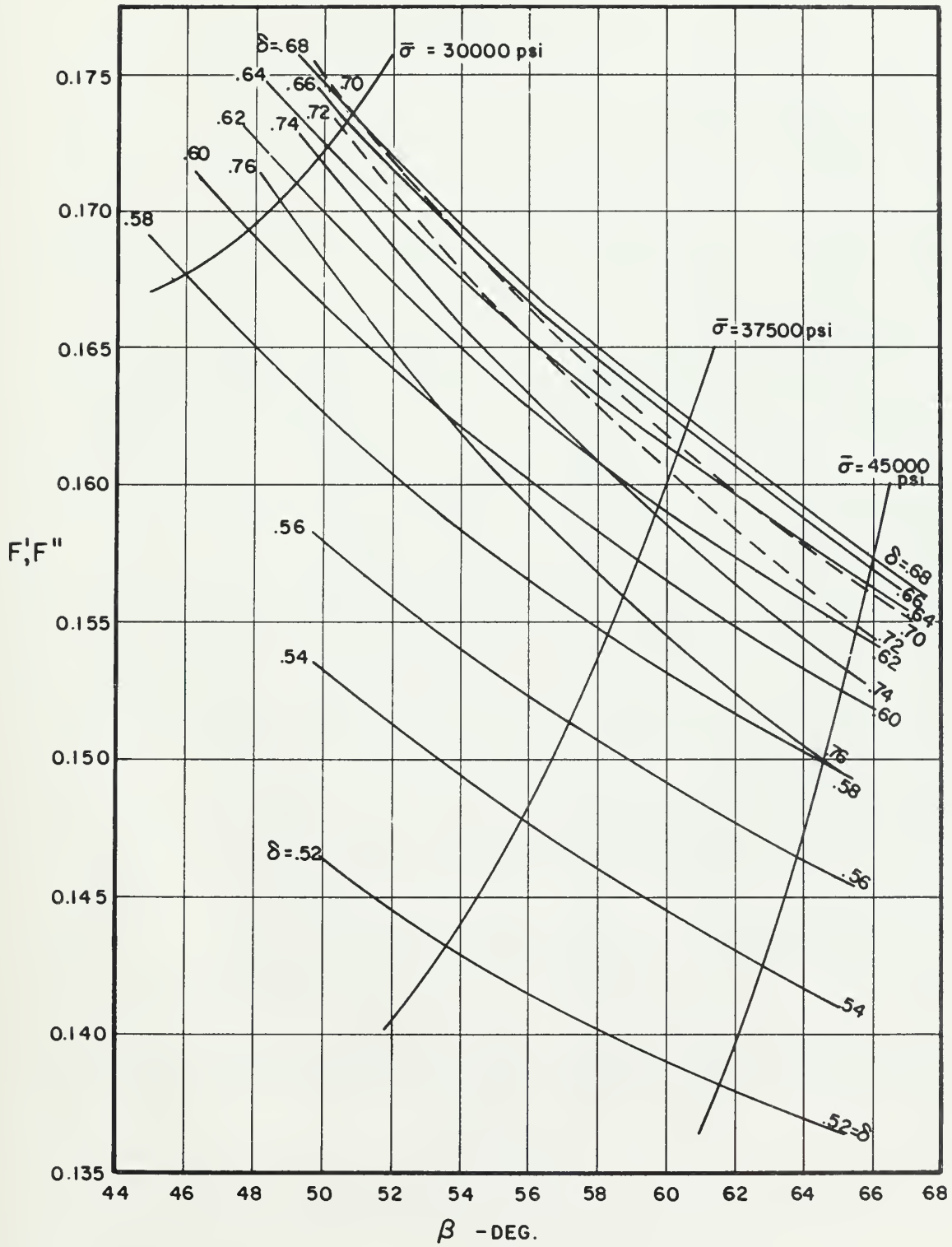

Figure 10. F' and F" Functions for Turbine Design Problem.

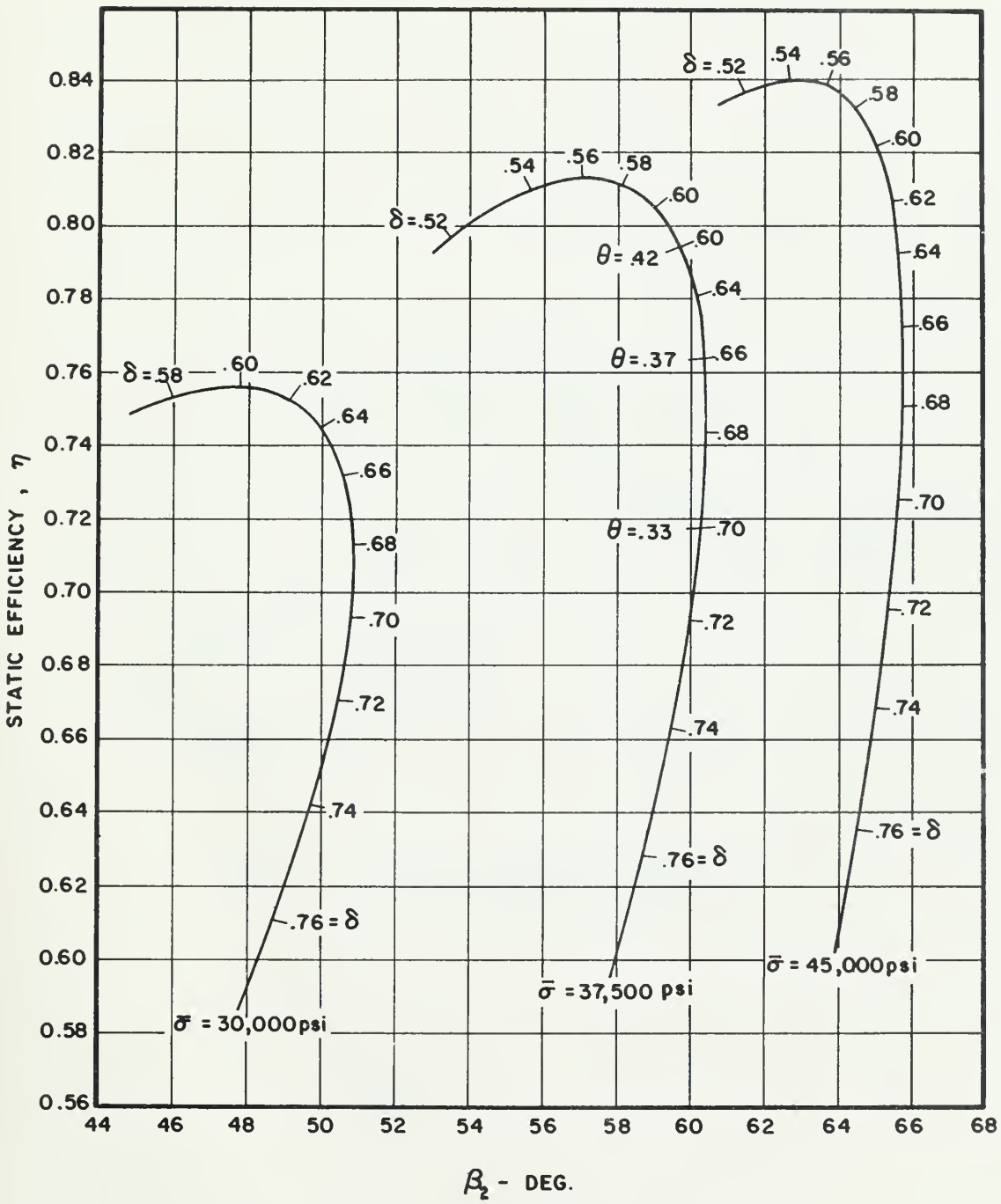

Figure 11. Constant Stress Efficiency Curves for Turbine Design Problem.

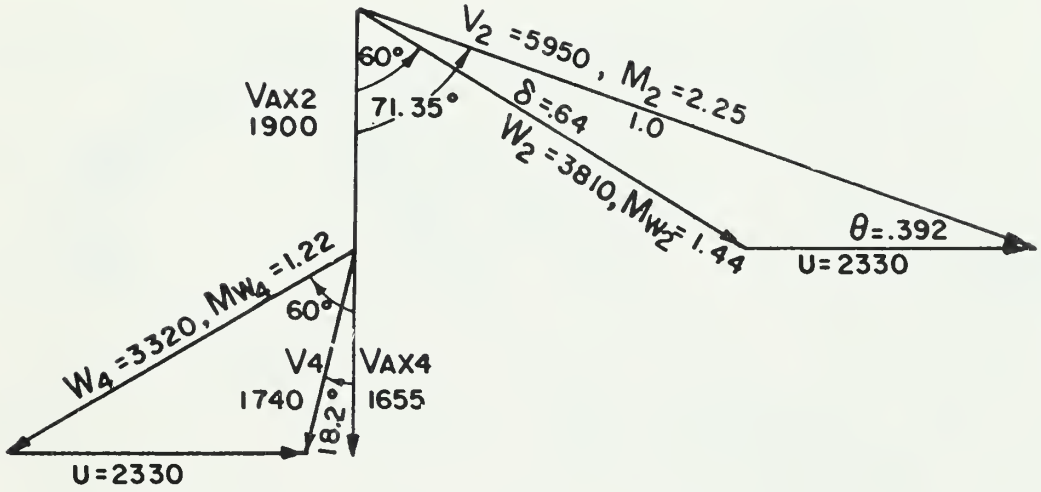

Figure 12. Design Velocity Triangle - Mean Radius Conditions.

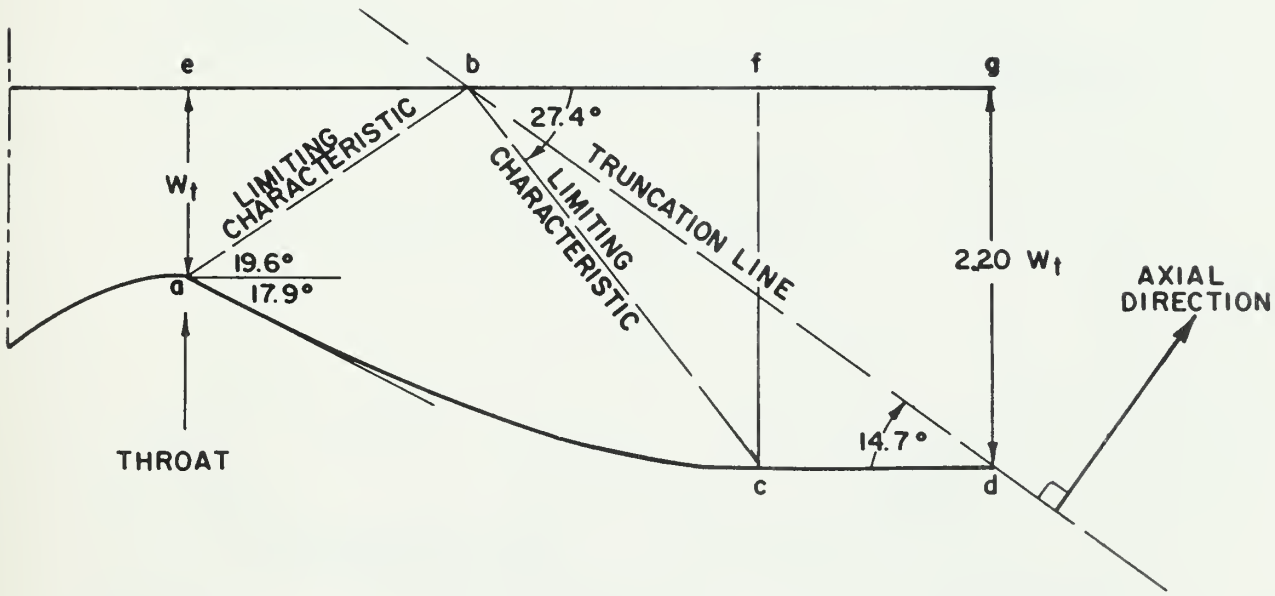

Figure 13. Sharp-Corner Nozzle Geometry Considerations.
(Not to Scale)

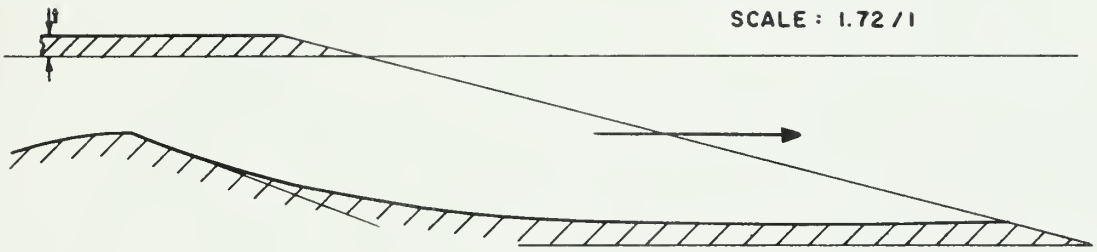

Figure 14a. Design Nozzle Profile.

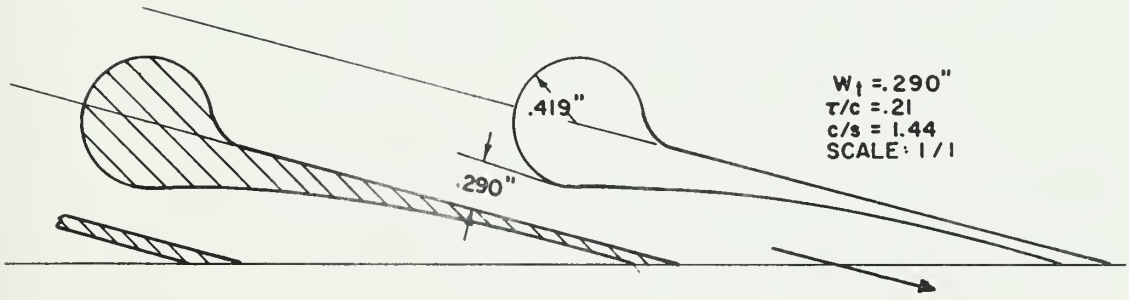

Figure 14b. Sharp-Corner Nozzle Cascade

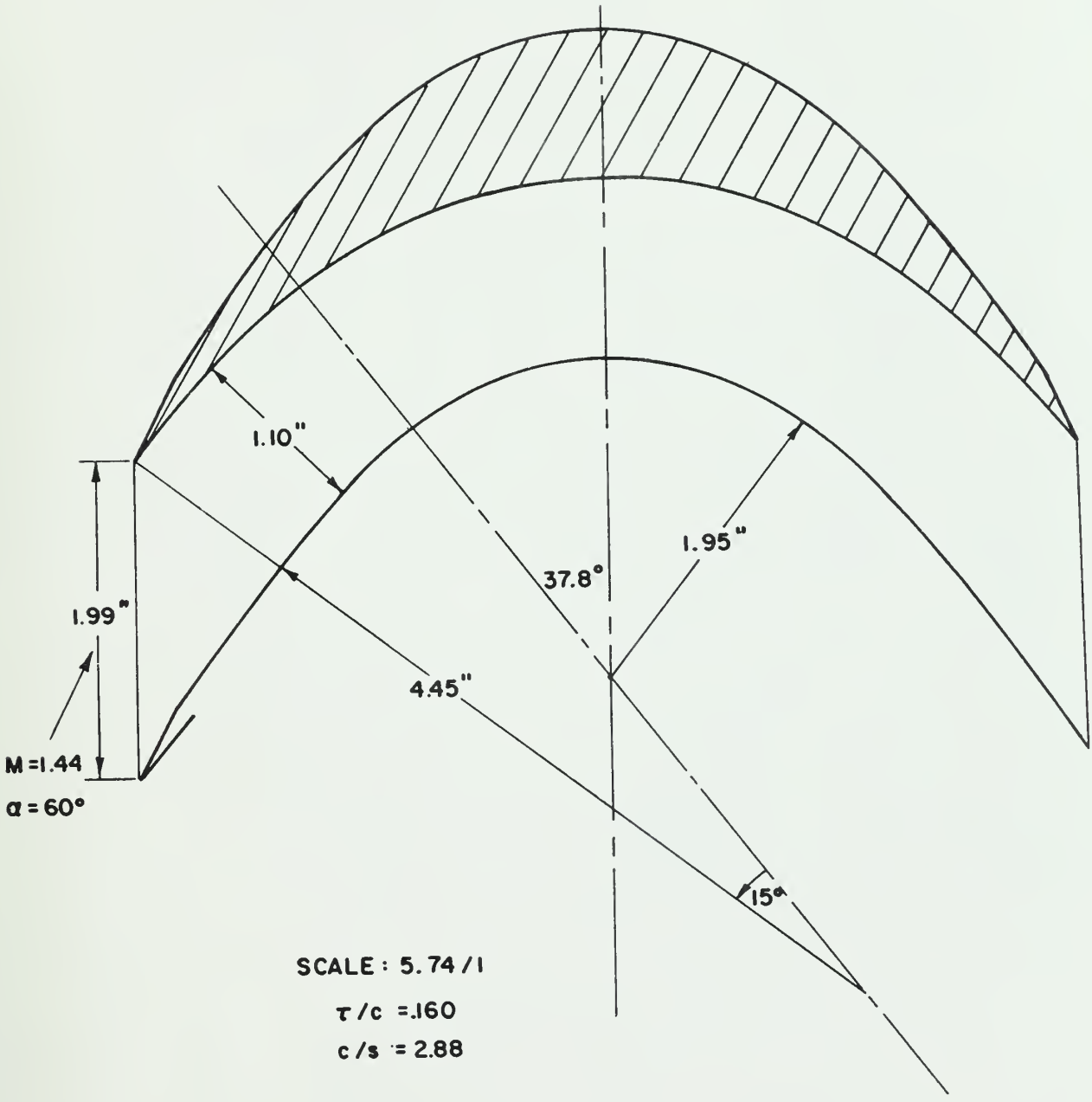

Figure 15. Design Rotor Profile.